Continental Shelf Research 169 (2018) 1–16

Contents lists available at ScienceDirect

Continental Shelf Research

journal homepage: www.elsevier.com/locate/csr

Research papers

Forerunner storm surge under macro-tidal environmental conditions in shallow coastal zones of the Yellow Sea

Seung-Won Suh[a,*], Hwa-Young Lee[b]

[a] Department of Ocean Science and Engineering, Kunsan National University, Daehak-ro 1170, Kunsan, Jeonbuk, Republic of Korea
[b] Disaster Information Research Division, National Disaster Management Research Institute, Jongga-ro 365, Jung-gu, Ulsan, Republic of Korea

ARTICLE INFO

Keywords:
Yellow Sea
Forerunner surge
Kelvin waves
Geostrophic setup
Resonance
Nonlinear effects

ABSTRACT

Typhoons affecting the west coast of Korea (WCK) in the Yellow Sea (YS) typically enter the continental shelf across the Ryukyu Islands, where surges can develop in the shallow water and interact with the macro-tidal environment. In this study, we investigate the generative mechanism of forerunner surge (FS) occurring before the main surge of two typhoons in the WCK, Prapiroon, and Bolaven. Sensitivity analyses of FS generation to bottom friction, Coriolis effects, tides, wind, and pressure forcing were conducted. The effect of the Coriolis force, which depends on latitudinal position, is not an influential factor in the FS along the shallow inner shelf of the WCK. However, Kelvin waves move along the WCK and cause nonlinear characteristics that amplify or dampen the FS, depending on the timing of flooding or ebbing tides. We found that the FS appeared at least 12.6 h prior to the main surge, which is almost the same as the geophysical resonance period. Moreover, the FS was not only influenced by the geostrophic setup, represented by the distance from the coast, but may also be amplified by topographic effects, such as the concavity of the coastline. When a typhoon enters the Ryukyu Islands at an angle $< 20^{\circ}$ and moves at a relatively slow speed ($< 20\,\mathrm{km\,h^{-1}}$), a FS is more likely to occur.

1. Introduction

As global climate change progresses, coastal hazards have increased, and therefore the need for mitigation or preparedness for storm surges has also risen (Hoffman et al., 2010; IPCC, 2011). During the storm season, meteorological agencies mostly announce possible peak surge height (SH) values when tropical cyclones are approaching coastal regions. However, surges occasionally occur 12–24 h prior to the main surge with significant water surface anomalies. Probabilistic modeling alone cannot capture these precedent surges, also termed forerunner surges (FS). Sometimes, the SH of FSs exceeds that of normal storms, as observed for Hurricane Ike, which had a SH of 1.7–2.5 m in Galveston Bay, Texas in 2008 (Hope et al., 2013).

Hurricane Ike gained public and scientific attention because it had a similar strength, track, and forward speed as Hurricane Rita in 2005; however, it exhibited quite different surge processes. Due to its large size and strong shore-parallel shelf current, Hurricane Ike generated the largest recorded geostrophic setup or forerunner (Kerr et al., 2013a, 2013b). Kennedy et al. (2011) explained that a large and unpredicted increase in water level appeared along a prominent section of the western Louisiana and northern Texas (LATEX) coasts 12–24 h before the landfall of Hurricane Ike. In some areas, water levels reached 3 m above mean sea level. However, SHs reaching 3 m occurred prior to the main surge, and could not be predicted by prevailing probabilistic analyses.

Hurricane Ike demonstrates that predicting FSs is extremely important for storm preparedness. Real-time guidance systems, such as the Coastal Emergency Risks Assessment (CERA, http://coastalemergency.org), employ deterministic simulations, which can provide estimates of maximum SHs. The deterministic approach can provide not only

Abbreviations: ADCIRC, Advanced Circulation Model; ASGS, Advanced Surge Guidance System; ATCF, Automated Tropical Cyclone Forecasting System; CERA, Coastal Emergency Risks Assessment; DH, Daeheuksando; EWS, Early Warning System; ECS, East China Sea; FES2012, Finite Element Solution 2012; FS, Forerunner Surge; GSHHG, Global Self-consistent, Hierarchical, High-resolution Geography Database; GOM, Gulf of Mexico; IC, Incheon; IPCC, Intergovernmental Panel on Climate Change; KHOA, Korea Hydrographic and Oceanographic Administration; KMA, Korea Meteorological Agency; KO, Kunsan outer port; MP, Mokpo; LATEX, Louisiana and Northern Texas; NGDC, U.S. National Geophysical Data Center; NWP, Northwestern Pacific; PS, Primary Surge; RDAPS, Regional Data Assimilation and Prediction System; RMW, Radius of Maximum Wind speed; SH, Surge Height; SP, Seogwipo; UTC, Universal Time Coordinated; WCK, West Coast of Korea; WSE, Water Surface Elevation; YS, Yellow Sea

* Corresponding author.
E-mail address: suh@kunsan.ac.kr (S.-W. Suh).

https://doi.org/10.1016/j.csr.2018.09.007
Received 13 June 2017; Received in revised form 18 July 2018; Accepted 16 September 2018
Available online 18 September 2018
0278-4343/ © 2018 Elsevier Ltd. All rights reserved.

maximum SHs, but also the heights of the FS or later surges according to updated meteorological databases of typhoons or hurricanes (Suh et al., 2015). Adopting a deterministic storm surge model may allow time-variant forecasts of both the main surge and FS as an advantage over the probabilistic approach. To aid in storm preparedness, early warning systems, such as the Advanced Surge Guidance System (ASGS), can be incorporated into the emergency management framework.

Storm phenomena are both time-variant and site-specific; thus, it is important to understand the ambient tidal hydrodynamics of a given region of interest. Thiebaut and Vennell (2011) analytically demonstrated that a combination of the storm translation speed (relative to depth), timescale, and direction could generate a resonant response in the ocean, and enhance storm surges as the disturbance crosses a vertical coast, step, or shelf. Wolf (1981) and Bertin et al. (2012) argued that the effects of shallow water are important in surge analysis for tidal ranges larger than 3 m and water depths below 10 m. Many secondary factors influence the magnitude of a storm surge through the Coriolis effect in the form of coastal upwelling and forerunners. While these factors may be secondary to winds in generating surges, they can be of great importance under certain storm conditions and coastal environments (Veeramony et al., 2012). Studies on the primary mechanisms underlying the generation of forerunners (Hope et al., 2013; Kennedy et al., 2011; Sebastian et al., 2014) have found that geometrical characteristics, Ekman setup, and size of the wind field can affect the FS height by ~1 m. Factors controlling the Coriolis-driven early setup include the cross-shelf wave, which has an approximate period coinciding with the resonant period of the shelf and coastally trapped Kelvin waves.

Resonant coupling between typhoons, tides, and topography accounting 12.6 h of the natural period of the Yellow Sea (YS) contributed to further enhancement of the storm surge in Typhoon Bolaven (Kim et al., 2014). The YS is a semi-enclosed marginal sea in the northwestern Pacific Ocean that is surrounded by the Korean Peninsula, the Chinese coast, and the Ryukyu Islands. Careful analysis of the conditions required to understand typhoon storm surges on the west coast of Korea (WCK). The WCK has a complex coastline marked by a very shallow depth. The macro-tidal environment ranges from a 3 m mean tidal range at Mokpo near the southwestern-most end, to a 9 m range at Incheon, located near the middle of the peninsula. Along the Korean coastlines, especially the WCK, FS occasionally appears at least 12.6 h prior to the primary surge (PS) of a typhoon.

In this study, we analyzed storm surges on the WCK addressing the importance of nonlinear effects on tide-surge interactions in shallow water areas with a macro-tidal range (Wolf, 2009). We also investigated Kelvin waves, resonance, and the effects of geostrophic setup when typhoons enter the continental shelf of the East China Sea (ECS) to the YS, passing over the Ryukyu Islands. Barotropic simulations of surges were conducted in order to identify the sensitivity of FSs to various factors, such as the Coriolis force, tides, and bottom friction, and we compared our findings to the dynamics of FSs in the Gulf of Mexico (GOM).

2. Characteristics of recorded forerunners on the west coast of Korea (WCK)

In general, three or four typhoons threaten Korea during the summer, from July to September each year. Typhoons occasionally occur during the perigean spring tide when the tidal range reaches the annual maximum. Fluctuations in the water level during this period can easily lead to the inundation of low-lying coastal areas. Analyzing historical typhoon track data, Kim and Suh (2016) found that ~41.2% of the typhoons impacting Korea affect the west coast, and could be amplified or altered by the geophysical setup, and/or strong alongshore tidal currents induced by meso- to macro-tidal environments.

In this study, two typical typhoon tracks passing the ECS and YS, Typhoons Prapiroon (TY0012) and Bolaven (TY1215) were selected to analyze FSs occurring due to geostrophic effects in the WCK. According to the best tracks, Prapiroon traveled northwest, and the wind field strengthened until it reached a 10 min sustained wind speed of 36 m s^{-1} and a radius of 290 km. Similarly, Typhoon Bolaven traveled north, and the wind field intensified until it reached a 10 min sustained wind speed of 64 m s^{-1} and a radius of 240 km. The maximum winds were 34 kt at

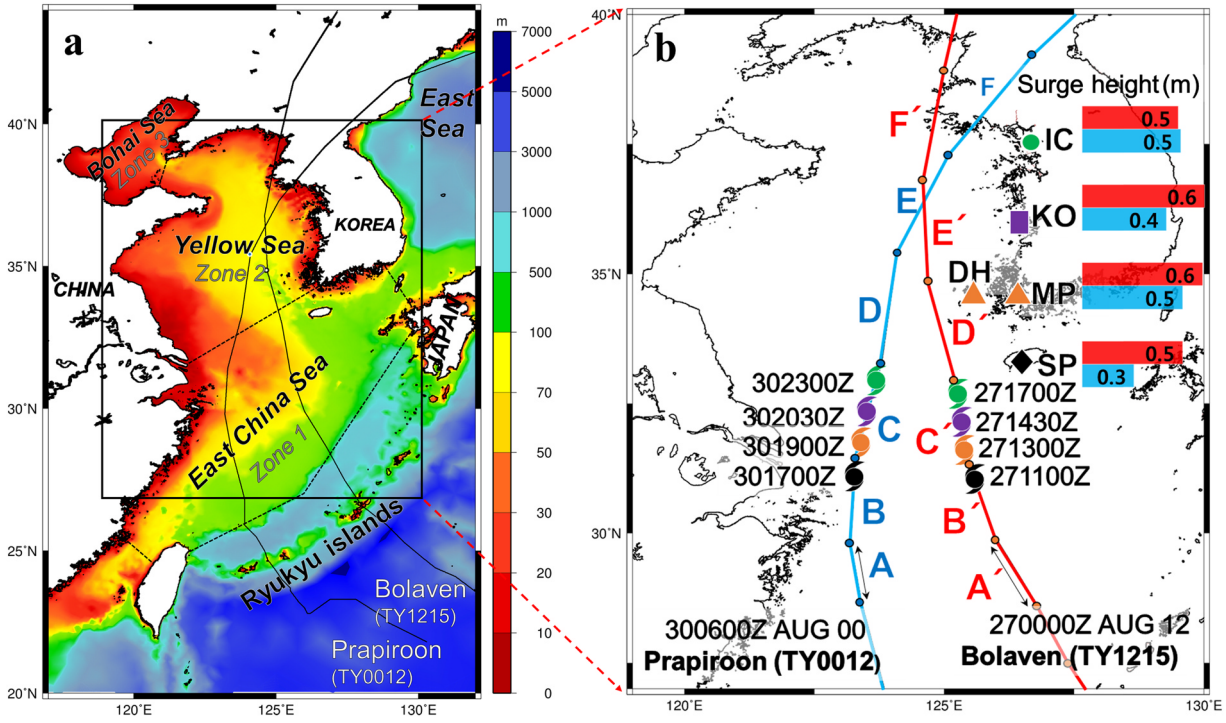

Fig. 1. (a) Typhoon tracks of Prapiroon and Bolaven passing the Ryukyu Islands. (b) The location of Prapiroon (blue line) and Bolaven (red line) when the FS reached the corresponding colored tidal station. The FS heights at the four stations are also shown.

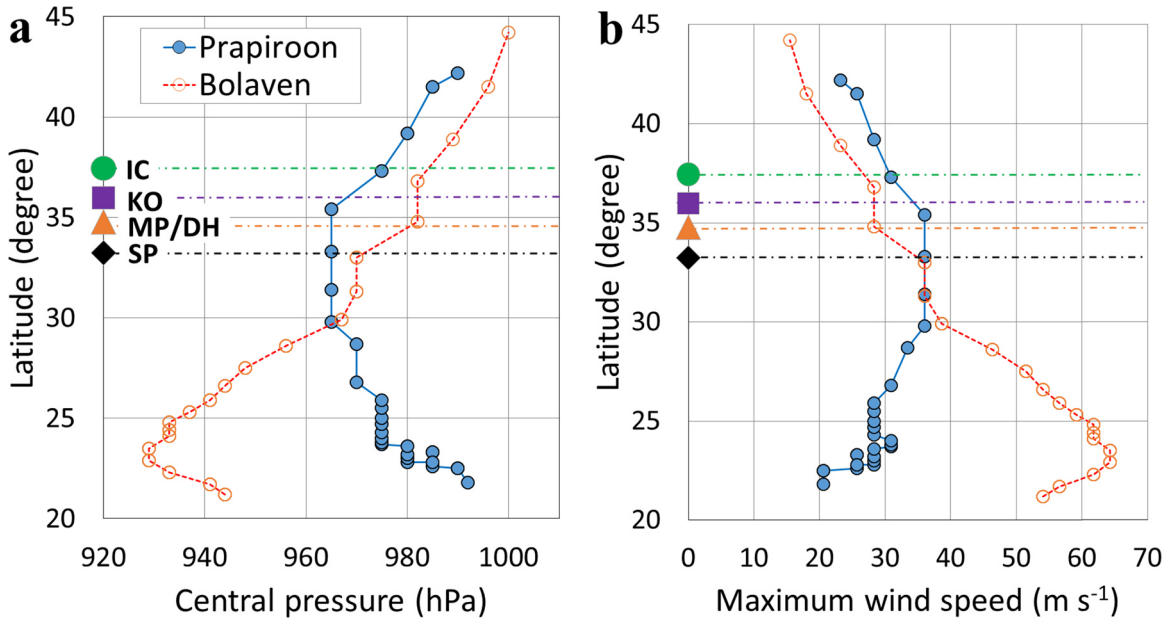

Fig. 2. Central pressure (a) and maximum wind speed (b) variations with respect to latitudes (corresponding tidal stations are denoted in the vertical axis) for Typhoons Prapiroon and Bolaven.

Table 1
(a) Typhoon movement speeds for the segments A to F (Prapiroon) and A′ to F′ (Bolaven), (b) FS surge occurrence time as hours since passing the Ryukyu Islands, (c) FS movement speed along the WCK, and (d) Free Kelvin wave speed ($\sqrt{gh}$) with mean depth for the zones ECS, YS, and Bohai Sea as shown in Fig. 1.

a	Typhoon moving speed (km h^{-1})	A	B	C	D	E	F
	Prapiroon	21	30	36	39	38	42
	Bolaven	27	27	32	34	37	39
b	Forerunner surge occurrence time	SP	MP	KO	IC		
	Prapiroon (300600Z AUG 00)	+ 11 h (301700Z)	+ 13 h (301900Z)	+ 14.5 h (302030Z)	+ 17 h (302300Z)		
	Bolaven (270000Z AUG 12)	+ 11 h (2701100Z)	+ 13 h (271300Z)	+ 14.5 h (271430Z)	+ 17 h (271700Z)		
c	FS moving speed (km h^{-1})	SP-MP	MP-KO	KO-IC			
	Prapiroon	87	68	18			
	Bolaven	87	68	18			
d	Kelvin wave speed (km h^{-1})	Zone 1 (East China Sea)	Zone 2 (Yellow Sea)	Zone 3 (Bohai Sea)			
		98	74	48			

1500 UTC on 31 August 2000 for Prapiroon and at 1500 UTC on 28 August 2012 for Bolaven, when the center of each storm was approximately 300 km from the coast. The tracks of the two typhoons and locations with time in UTC are depicted in Fig. 1. The central pressure and maximum wind speed variations with respect to latitude are plotted in Fig. 2. In Table 1, the moving speeds of the typhoons, the FS waves between selected locations, and the mean Kelvin wave speeds are listed. Free Kelvin wave speed was computed as the traveling speed of the shallow water surface gravity wave, accounting for mean depth of the corresponding three coastal zones (Fig. 1a). Analyzing these geophysical characteristics can inform the potential for future FS occurrences in the WCK.

To analyze sea surface fluctuations, one-minute data for Bolaven were reproduced as hourly water levels to make it consistent with the hourly recorded data of Prapiroon from major tidal stations using a Tidal Analysis Software Kit (TASK-2000; Bell et al., 1999), encompassing 63 tidal constituents based on tidal record data archived by the Korea Hydrographic and Oceanographic Administration (KHOA, www.khoa.go.kr). Water level anomalies for major tidal stations, Seogwipo (SP), Daeheuksando (DH), Mokpo (MP), Kunsan outer port (KO), and Incheon (IC) are shown in Fig. 3. At each station, FSs normally appeared 12 h (moving from SP to IC) before the typhoons passed. Even though the FSs of both typhoons had the same magnitude (0.5 m) at IC, different primary SHs were recorded (1.17 m for Prapiroon and 1.52 m for Bolaven). It should be noted that any small water surface anomaly coinciding with high tides may produce severe coastal hazards due to the macro-tidal environment characterized by 9 m mean spring tidal range at IC (Suh et al., 2014). Especially during the time of perigean spring tide, tidal ranges vary from 0.07 m to 9.26 m, and the 0.5 m FS height increased the high water elevation to 9.76 m (Fig. 3a). Though Typhoon Prapiroon had a maximum SH of 1.17 m at IC, it did not cause any major damage because it coincided with the low tide. However, due to the FS occurring during high tide, the coastal area immediately south of IC was inundated. Although the inundation depth and area were not clearly recorded, local cable news broadcasted the unusual event. The main reason for the resulting disaster was that insufficient attention was given to the FS by the forecasting agency, the Korea Meteorological Agency (KMA).

3. Storm surge model and set-up conditions

One of the aims of this study was to enhance the reliability of near real-time forecasting of storm surges, including FSs. For this purpose, the ADCIRC model (Luettich et al., 1992) was applied and compared with recorded data. The ADCIRC model is an unstructured, two-dimensional, depth-integrated, or three-dimensional ocean circulation model, and is one of the most widely used models in coastal and ocean simulations. It has been verified and validated for hurricanes in the

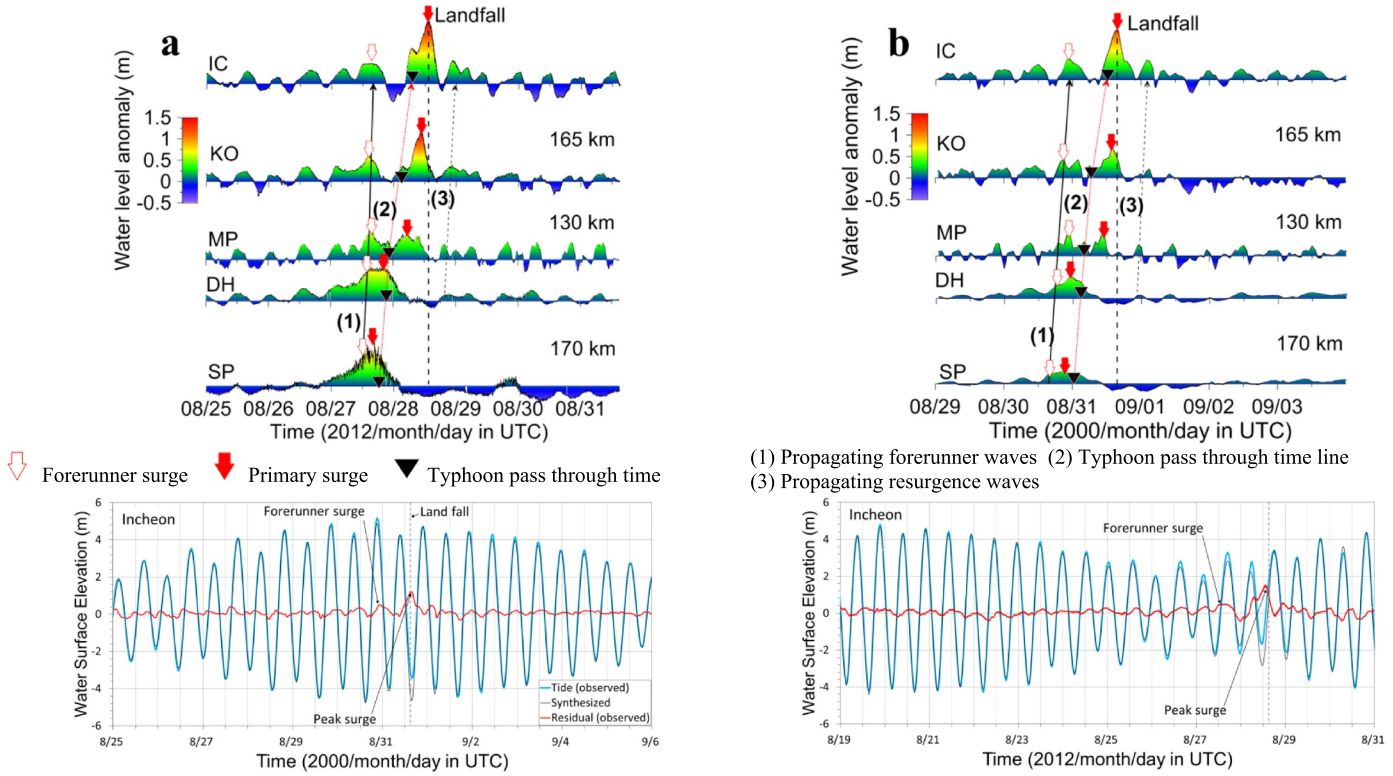

Fig. 3. (a) Water level anomalies at selected stations moving from the low latitude (SP) to high latitude (IC) for Typhoons Prapiroon (upper panel) and comparison of observed, synthesized tide, and surge elevation variation (lower panel), and (b) for Typhoon Bolaven. FSs are marked as open arrows, and primary surges are denoted as red filled arrows. The vertical spacing represents the unscaled distances between recording stations. Propagation of the FS and duration of the passage at the same latitude for each station are shown as solid black lines and red dotted lines, respectively.

GOM in hindcasting studies (Blanton et al., 2012; Dietrich et al., 2011; Kennedy et al., 2011; Westerink et al., 2008; Weaver and Slinn, 2004).

The advantage of utilizing unstructured grids to model the Korean coast, especially the WCK, which has a complex coastline and shallow depth, is that they can capture very sophisticated coastal hydrodynamics, such as nonlinear shallow water tide and surge interactions. In this study, we exploited an existing efficient model and applied the finite element grid, NWP-G57k, which covers the northwestern Pacific (NWP) sea with a total of 56617 nodes (Suh et al., 2015). This grid structure was developed for near real-time forecasting of storm surges using ADCIRC, with the minimum node spacing of 100 m along the Korean Peninsula, and a maximum node spacing of 140 km near the open boundary (Fig. 4). This was considered sufficient to represent the topography along the Korean coast. Coarser grid structures can be applied to early-warning systems with greater computational efficiency than finer grids. Thus, to determine the effects of grid refinement on FS prediction, we additionally tested the grid systems NWP-G116k and NWP-G258k (Table 2).

In the configuration of the numerical model, the topology of the shallow macro-tidal coast along the WCK was well represented to reflect the nonlinear interactions between rising tides and typhoon-induced currents during the spring tide period. Strong tidal currents may act as an enhancing factor when coinciding with typhoon-induced flows. In addition, numerous sensitivity tests were performed during model configuration for geostrophic parameters, such as translation speed V_s, radius of vortex wind R, and distance of typhoon tracks from the coast, D_s. Details of the sensitivity tests are discussed in Section 4.2 and tabulated in Tables 4, 5.

The ETOPO1 (Amante and Eakins, 2009) was adopted for the bathymetry of the NWP and YS (Suh et al., 2015). Near the Korean coast, detailed local bathymetry data were also considered. The coastline was extracted from a worldwide shoreline database, the Global Self-consistent, Hierarchical, High-resolution Geography Database (GSHHG) of the U.S. National Geophysical Data Center (NGDC; Wessel and Smith, 1996). For the open boundary conditions, which act as the driving force for the tidal model, eight major tidal constituents, (M_2, S_2, K_1, O_1, N_2, P_1, K_2, and Q_1) extracted from the finite element solution 2012 (FES2012) tidal model (Carrère et al., 2012) were applied. Since vortex shape plays an important role in storm surge simulation (Mattocks and Forbes, 2008; Suh et al., 2015; Xie et al., 2006), we implemented several vortex shapes in formulating the surge model to determine its impact on FS computation.

In validating the FS and storm surge prediction, target typhoons were simulated for at least 20 days, including 15 days of spin-up and hot start, wherein the last five days were devoted to forerunner and surge simulations. For efficient computation, a system with a total of 64 Intel Nehalem cores with 2.4 GHz processing speed was used along with Mellanox's Infiniband (19 Gbps bandwidth) for high-speed communication between parallel computing nodes.

4. Numerical simulations of forerunner surges (FSs) and sensitivity analyses

Forerunner surges (FSs) often occur when a typhoon path at some distance from the coast moves at approximately the same speed as a Kelvin wave. In this study, numerical simulations emphasizing geostrophic balance and bathymetry were performed to determine the most important factors affecting the FS and PS. To capture the primary forcing in FS generation, several tests were conducted, each neglecting one forcing term in the momentum equation (Eq. (1)). In addition, sensitivity tests for typhoon wind fields and moving characteristics were also performed to analyze the importance of meteorological effects on FS generation.

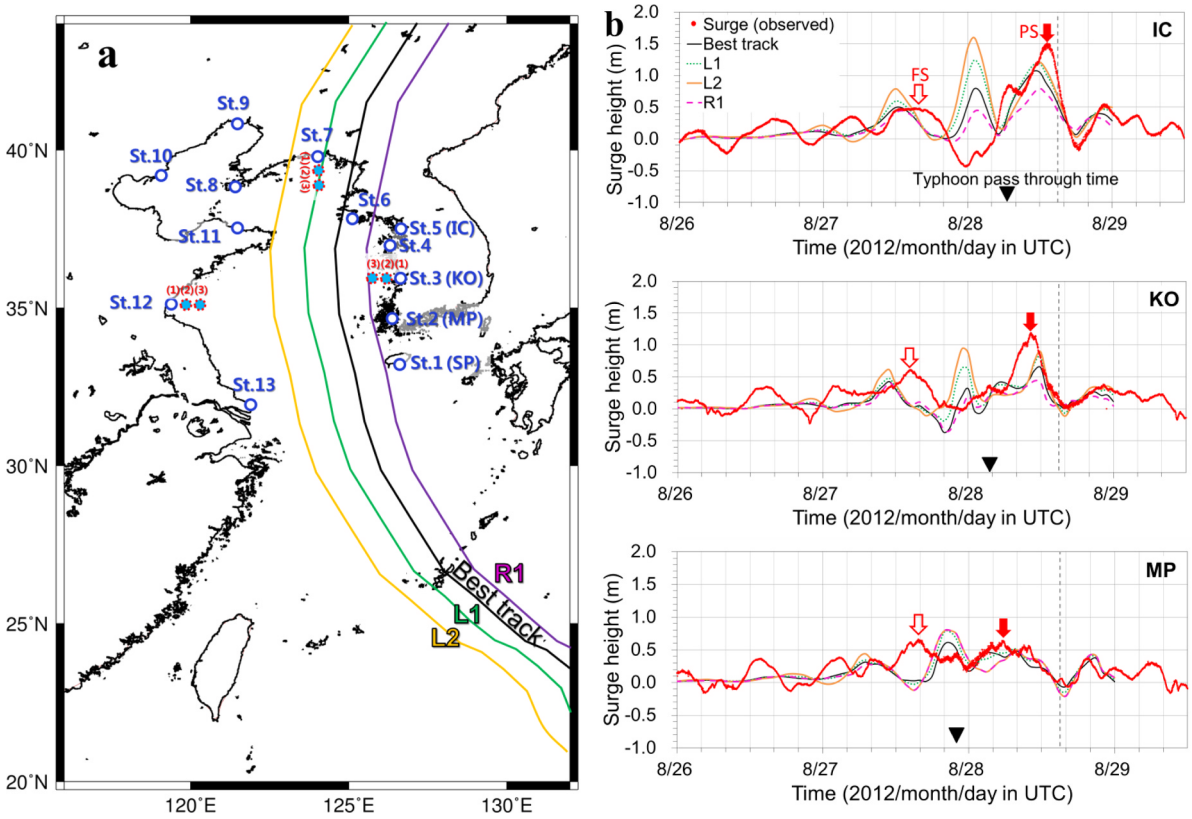

Fig. 4. Sensitivity tests on distance of the FS and PS in case of Typhoon Bolaven (a) assigning hypothetical tracks with 1 degree of longitude separation distances shifting to left and right with respect to best track. Station numbers along the Korean and Chinese coast denotes for Kelvin wave propagation. (b) Comparison of simulated FS and PS heights at selected recording stations. The dashed vertical line represents landfall time.

Table 2
Details of grid structure tested in storm surge modeling (Suh et al., 2015).

		NWP-G		
		57 k	116 k	258 k
No. of nodes		56,617	116,620	258,046
No. of elements		104,094	206,416	484,505
Min. grid spacing (m)		103	161	113
Nodal density (%)	depth < 10 m	40.4	47.2	37.5
	10–20 m	17.4	16.8	14.5

4.1. Equations for geostrophic flow and Ekman transport

The shallow water momentum equation can be described in terms of its components, where L is local acceleration, A is advection, Z is the surface gradient, P is atmospheric pressure, C is the Coriolis force, T is tidal potential, S is the surface and bottom stress, and D is diffusion, as shown in Eq. (1) (Kerr et al., 2013b).

$$\underbrace{\frac{\partial \mathbf{u}}{\partial t}}_{L} + \underbrace{\mathbf{u}\cdot\nabla\mathbf{u}}_{A} = \underbrace{-g\nabla\zeta}_{Z} \underbrace{-\frac{\nabla p}{\rho}}_{P} \underbrace{-f\times\mathbf{u}}_{C} + \underbrace{g\nabla\alpha\eta}_{T} + \underbrace{\frac{\tau_s-\tau_b}{\rho H}}_{S} + \underbrace{\frac{\mathbf{M}}{H}}_{D} \quad (1)$$

where $\mathbf{u}$ represents the depth-averaged velocity, t is time, f is the Coriolis parameter, ρ is the density of sea water, g is gravitational acceleration, ζ represents the free surface departure from the geoid, p represent the atmospheric pressure at the sea surface, α is the Earth elasticity reduction factor, η is the Newtonian equilibrium tide potential, τ_s accounts for the imposed surface stresses for winds and waves, τ_b represents the bottom stress, H is the water column height, and $\mathbf{M}$ represents lateral stress (Kerr et al., 2013b). Calculation of the driving forces, atmospheric pressure, tidal potential, wind stress, wave radiation stress gradient, and bottom stress depends on the quality of the input data and the model parameterization, whereas the local acceleration, advection, Coriolis force, and surface gradient components are only responsive to the driving terms (Kerr et al., 2013b).

Ignoring driving terms and nonlinear effects result in the geostrophic balance equation (Eq. (2)). Eq. (3) represents the geostrophic balance equation due to Earth's rotation, shown in the x-direction.

Table 3
Separation distance effect on SHs at selected stations shown in Fig. 4.

Track	IC				KO				MP			
	FS		PS		FS		PS		FS		PS	
	m	%	m	%	m	%	m	%	m	%	m	%
R1	0.45	− 8	0.80	− 25	0.40	− 5	0.41	− 36	0.28	− 10	0.79	30
Best track	0.49		1.07		0.42		0.64		0.31		0.61	
L1	0.60	22	1.24	16	0.48	14	0.89	39	0.34	10	0.79	30
L2	0.79	61	1.60	50	0.61	45	0.94	47	0.44	42	0.79	30

Table 4
Comparison of variations in the FS and PS for Typhoons Prapiroon(P) and Bolaven(B), neglecting the momentum terms.

Momentum term	SH(m), *variation (%)*	IC				KO				MP			
		FS		PS		FS		PS		FS		PS	
		P	B	P	B	P	B	P	B	P	B	P	B
Best track (reference)	SH	0.67	0.49	1.59	1.07	0.49	0.42	1.61	0.64	0.64	0.31	1	0.61
Tide off	SH	0.81	0.43	1.22	0.98	0.59	0.33	0.9	0.51	0.48	0.31	0.88	0.57
	Variation	*21*	*− 12*	*− 23*	*− 8*	*20*	*− 21*	*− 44*	*− 20*	*− 25*	*0*	*− 12*	*− 7*
Wind off	SH	0.12	0.01	0.28	0.28	0.12	0.02	0.55	0.35	0.14	0.06	0.37	0.31
	Variation	*− 82*	*− 98*	*− 82*	*− 74*	*− 76*	*− 95*	*− 66*	*− 45*	*− 78*	*− 81*	*− 63*	*− 49*
Pressure off	SH	0.15	0.5	0.76	0.76	0.27	0.42	0.45	0.42	0.30	0.29	0.34	0.38
	Variation	*− 78*	*2*	*− 52*	*− 29*	*− 45*	*0*	*− 72*	*− 34*	*− 53*	*− 6*	*− 66*	*− 38*

Integrating Eq. (3) with respect to x, obtains the linearized geostrophic setup height ξ (Eq. (4)), which reveals that sea surface elevation increases with increasing velocity v, distance from the coast D_S, and latitude ϕ.

$$\underbrace{f \times \mathbf{u}}_{C} = -\underbrace{\frac{\nabla p}{\rho}}_{P} \tag{2}$$

$$fv = \frac{1}{\rho}\frac{\partial p}{\partial x} \tag{3}$$

$$\xi = 2\Omega sin\phi v D_s \tag{4}$$

A geostrophic current is a current wherein the horizontal pressure gradient is in balance with the Coriolis force. Geostrophic balance assumes that momentum advection and frictional forces are small. Outside the equatorial band (where the Coriolis force is approximately equal to zero), geostrophic velocities u_g and v_g are given by Eqs. (5) and (6) (Sudre et al., 2013):

$$u_g = -\frac{g}{f}\frac{\partial H}{\partial y} \tag{5}$$

$$v_g = \frac{g}{f}\frac{\partial H}{\partial x} \tag{6}$$

where, y and x are the latitude and longitude, and all other parameters are those defined in Section 4.1. At the surface, it is necessary to account for wind-driven currents that result from the balance between the frictional wind stress and the Coriolis force. The Ekman regression model of the wind-driven current describes the following linear steady momentum balance, for the y- and x-directional wind stress fields, τ_{sy} and τ_{sx}:

$$fh_e u_e + r_e v_e = \frac{\tau_{sy}}{\rho} \tag{7}$$

$$-fh_e v_e + r_e u_e = \frac{\tau_{sx}}{\rho} \tag{8}$$

where h_e and r_e are the thickness of the Ekman layer and the linear drag coefficients, respectively (Sudre et al., 2013).

4.2. Geostrophic balance and Kelvin wave simulations

Simulations were performed to analyze the impact of two factors on the generation of FSs, the effect of distance from the coast, D_s, described in Eq. (4), and the effect of bathymetry, or the thickness of the Ekman layer, shown in Eqs. (7) and (8). To determine the influence of D_s on the FS, we simulated three tracks for Typhoon Bolaven, as shown in Fig. 4a. We assigned one track close to the coast and two farther from the coast by deviating by one or two degrees of longitude. The simulated results for the major stations, IC, KO, and MP, are shown in Fig. 4b. As expected, when the passage of the typhoon track moved farther from the coast, higher SHs occurred (Table 3). It should be noted that the peak surge appeared approximately one hour earlier for tracks that were farther away, that is, the SH corresponding to the L2 track occurred earlier than the R1 track, even though the magnitudes of the surges were similar. Moreover, the SHs at IC

Table 5
Comparison of FS and PS for Typhoons Prapiroon(P) and Bolaven(B), sensitivities with respect to vortex movement speed, wind field radius of 34 kt, and V_{max}.

	SH(m), *variation (%)*	IC				KO				MP			
		FS		PS		FS		PS		FS		PS	
		P	B	P	B	P	B	P	B	P	B	P	B
Best track (reference)	SH	0.67	0.49	1.59	1.07	0.49	0.42	1.61	0.64	0.64	0.31	1	0.61
Moving spd-20%	SH	0.68	0.52	1.6	0.97	0.58	0.5	1.67	0.77	0.60	0.32	1.07	0.53
	Variation	*1*	*6*	*1*	*-9*	*18*	*19*	*4*	*20*	*-6*	*3*	*7*	*-13*
Moving spd + 20%	SH	0.65	0.48	1.71	1.14	0.43	0.36	1.1	0.57	0.99	0.3	0.99	0.88
	Variation	*-3*	*-2*	*8*	*7*	*-12*	*-14*	*-32*	*-11*	*55*	*-3*	*-1*	*44*
Wind field-20%	SH	0.64	0.23	1.6	1.08	0.29	0.15	1.64	0.64	0.61	0.15	1	0.63
	Variation	*-4*	*-53*	*1*	*1*	*-41*	*-64*	*2*	*0*	*-5*	*-52*	*0*	*3*
Wind field + 20%	SH	0.81	0.82	1.6	1.07	0.69	0.75	1.6	0.75	0.70	0.48	1.01	0.59
	Variation	*21*	*67*	*1*	*0*	*41*	*79*	*-1*	*17*	*9*	*55*	*1*	*-3*
Vmax-20%	SH	0.49	0.6	1.52	1.04	0.38	0.5	1.57	0.62	0.73	0.34	1.01	0.61
	Variation	*-27*	*22*	*-4*	*-3*	*-22*	*19*	*-2*	*-3*	*14*	*10*	*1*	*0*
Vmax + 20%	SH	0.83	0.58	1.67	1.07	0.56	0.53	1.68	0.68	0.60	0.37	1.01	0.63
	Variation	*24*	*18*	*5*	*0*	*14*	*26*	*4*	*6*	*-6*	*19*	*1*	*3*
Symmetric vortex	SH		0.12		0.82		0.1		0.38		0.08		0.32
	Variation		*-76*		*-23*		*-76*		*-41*		*-74*		*-48*
Dynamic Asymmetric vortex	SH		0.12		1.23		0.17		0.54		0.14		0.56
	Variation		*-76*		*15*		*-60*		*-16*		*-55*		*-8*
Gridded wind vel. and pressure	SH		0.4		1.24		0.42		1.09		0.27		0.54
	Variation		*-18*		*16*		*0*		*70*		*-13*		*-11*

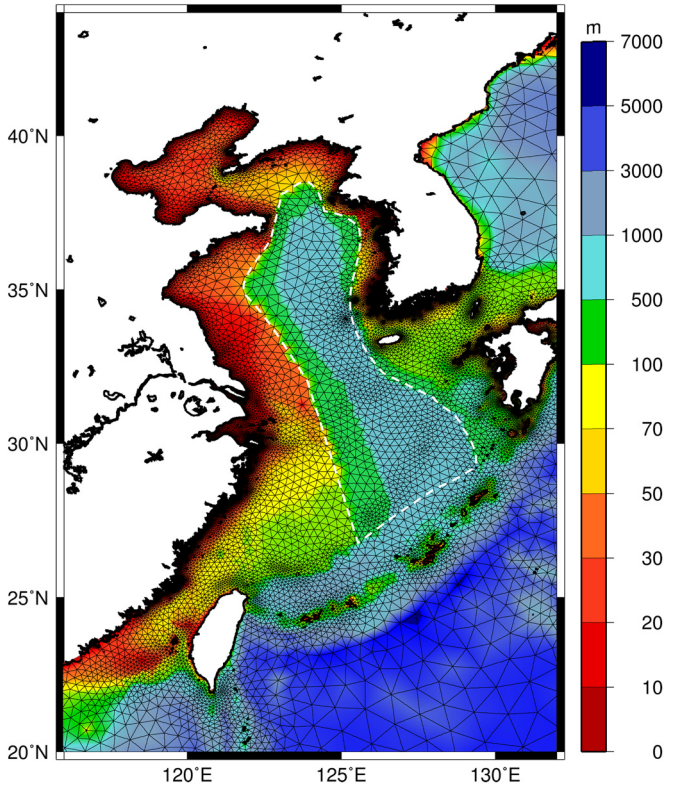

Fig. 5. Hypothetically deepened bathymetry of the YS up to 1000 m to test the Ekman layer effect.

station, which is the location closest to the landfall point, were higher than at stations KO and MP in these tests.

Simulations were also used to determine the impact of the thickness of the Ekman layer on the SH and FS. To investigate the importance of bathymetry, we compared the WCK during Typhoon Bolaven to LATEX during Hurricane Ike. The Ekman setup due to surface wind stress and rotational effects on the WCK could not be directly compared to LATEX because the GOM is significantly deeper than the YS. The Ekman layer is known to be spatially variable, but typically has a depth of at least several tens of meters. Hence, to make the two situations comparable, with the same order of magnitude, we artificially increased the depth of the YS in the simulation to 1000 m (Fig. 5). We then simulated the Ekman effect and compared the two regions.

We simulated the track of Typhoon Bolaven using the hypothetically increased depth. The FS and PS at IC and KO stations decreased while there was no distinct difference at MP station (Fig. 6). According to the overall simulated results, the response to the Coriolis effect on the artificially deepened YS exhibited a major trend of increasing water surface elevations during both FSs and PSs. The effect of the Coriolis force on SHs was dominant in the hypothetical simulations, indicating that the FS and PS are insensitive to the Coriolis force under the shallow depth conditions in the YS. Thus, the role of the Coriolis force on the generation of FSs and PSs appears to be less significant in shallow regions, such as the WCK as compared to deep regions, such as the GOM.

In addition to analyzing geostrophic effects on FS, the propagation characteristics of coastal trapped waves propagating were investigated. To capture the characteristics of Kelvin waves in this numerical simulation, spatio-temporal hydrographs were analyzed, focusing on the water surface elevation movement with the best track data of Typhoon Bolaven along the reference coastal points in Fig. 4. In the simulation, tidal effects were neglected to exclusively identify free wave propagation. The results reveal that Kelvin waves propagated counter-clock wise when the storm entered the continental shelf after crossing over the Ryukyu Islands (Fig. 7a); peak FS heights appeared at St.1 station, and then traveled northward. The free

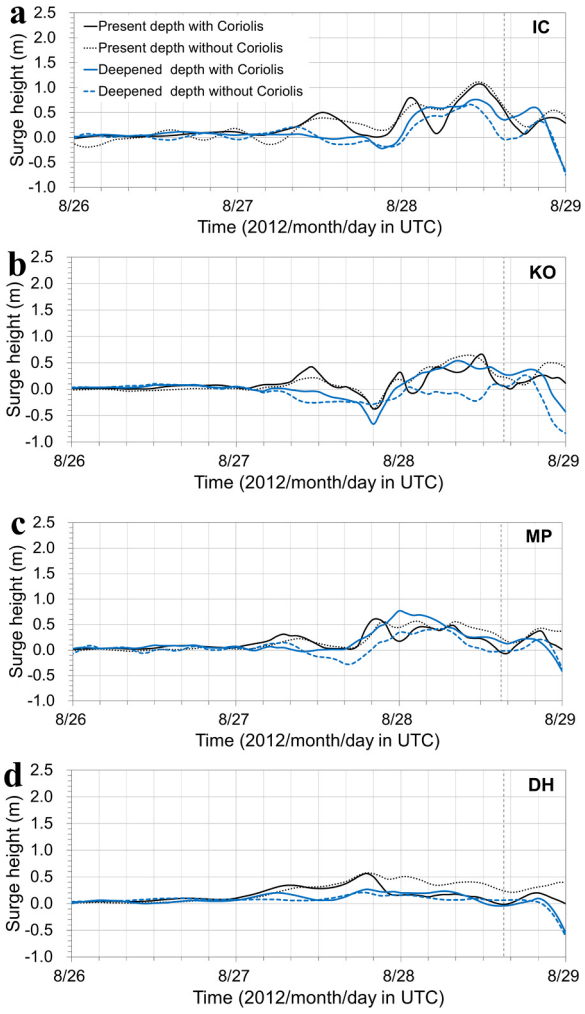

Fig. 6. Comparisons of the present depth and hypothetically deepened condition simulations of surge elevations in case of Typhoon Bolaven. WSE at major tidal stations (a – d) along WCK are plotted with/without Coriolis force term.

wave moved relatively faster in the YS, with a mean traveling velocity of 75 km h^{-1} (i.e., the gradient of the line connecting the FS crests, from St.1 to St. 8, is steeper) than that on the Bohai Sea (from St. 8 to St. 11) with a mean traveling velocity of 61 km h^{-1}. These simulated results reaffirm the observed FS characteristics as stated in Section 2 and listed in Table 1 because the mean depth of the YS is deeper than that of Bohai Sea. In addition to the coastally trapped pattern of Kelvin waves, we found the e-folding decay of wave height (Wang, 2002) in the offshore direction (Fig. 7b) for the three selected stations.

4.3. Sensitivity analysis for forcing factors

Understanding the nonlinear interactions of surges and tides in both horizontal and vertical directions in the macro-tidal environment is important. Thus, complex coastlines, tidal flats, and associated bottom friction were investigated in detail to represent complex tidal interactions, especially for the inner shelf basin of the YS as Lentz and Fewings (2012) indicated. To represent local bottom topography, a depth-dependent bottom friction coefficient was applied to account for the nonlinear frictional effect. In this study, bottom friction was treated in the form of Chezy's formulae (Eqs. (9) and (10)) to incorporate depth-dependent friction in the simulation. The base value for Manning's coefficient of 0.02 for regions with depths > 100 m was adjusted by ± 0.005 (20–25%) depending on water depth, and a coefficient of 0.025 was applied to most coastal areas of the YS. However, spatial variation was not considered in this study. The

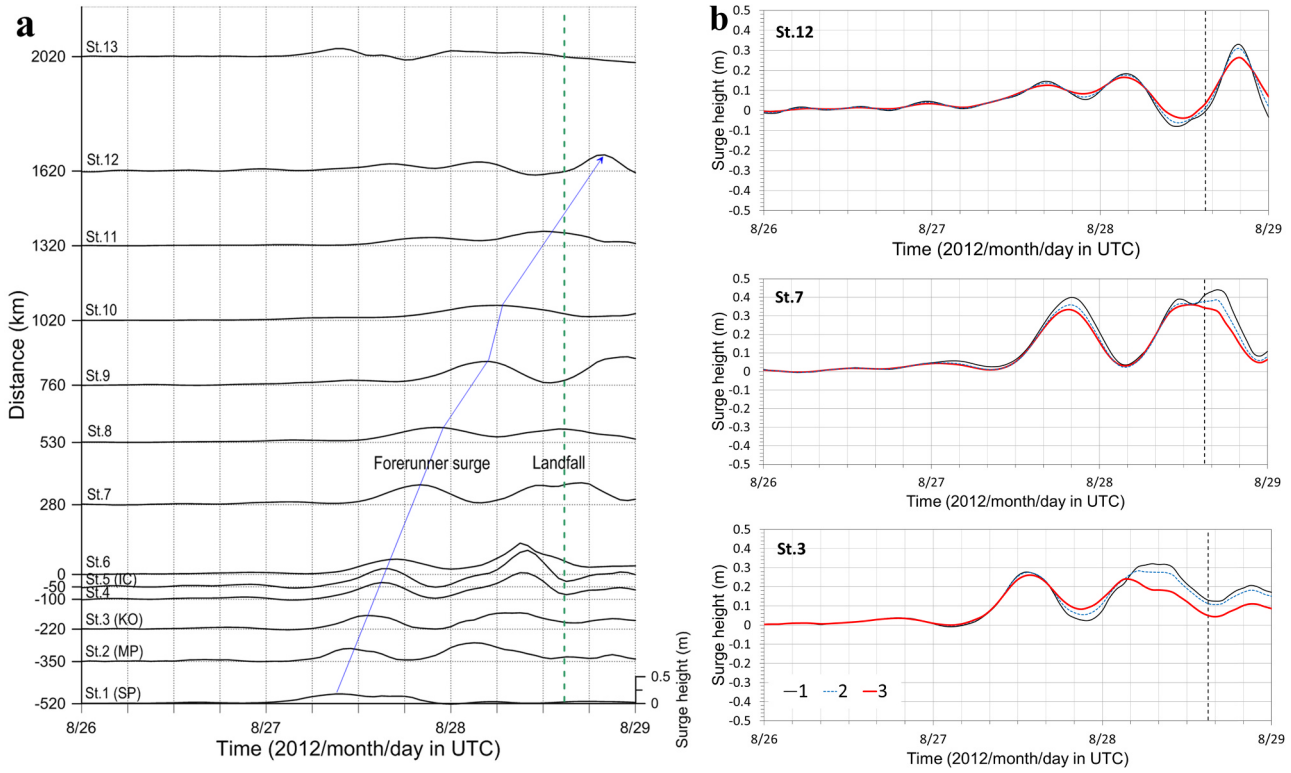

Fig. 7. Water surface anomalies induced by Typhoon Bolaven (a) at reference stations (St. 1 to St. 13) shown in Fig. 4, and (b) at three on-off shore points of St. 3, St. 7, and St. 12. The blue arrow line represents the Kelvin wave propagation along the stations.

computed results appeared to be insensitive at tidal stations SP and DH, which are islands and have a mean depth of 80–100 m. Conversely, the results at other onshore tidal stations were sensitive, with higher SHs with lower friction and lower heights with higher friction.

$$C_z = \frac{H^{\frac{1}{6}}}{n} \tag{9}$$

$$C_f = \frac{g}{C_z^2} = \frac{gn^2}{\sqrt[3]{H}} \tag{10}$$

where, C_z is Chezy's bottom friction coefficient, C_f is the bottom friction coefficient, and n is Manning's coefficient.

When typhoons of typical sizes move according to the geophysical Kelvin wave speed along the ECS to YS, FSs can occur. The Ekman setup along the WCK acts as a factor elevating SH when typhoons enter the YS. We used relatively simple momentum equations by neglecting one of the surface pressure or tide forcing terms, as in the studies of Kennedy et al. (2011) and Kerr et al. (2013b), to determine the most important influencing factor(s) for FS generation.

To determine the responses of FS, numerical results for IC, KO, and MP were analyzed for both typhoons. The FS and PS occurrence time and height variations for Prapiroon are shown in Fig. 8a–d and for Bolaven in Fig. 8e-h. The observed and best track simulation are shown with four simulation results, each neglecting one of the forcing terms: nonlinear tide, wind stress on the sea surface, and central pressure depression.

According to the recorded water elevations at the tidal stations, the FS appeared approximately 12 h prior to the Typhoon Prapiroon passing through KO and IC. However, it appeared 8 h prior to the passage through MP. The recorded FS heights were 0.49 m, 0.42 m, and 0.50 m at IC, KO, and MP, respectively. However, simulated results based on best track data exhibited a slight overestimation with values of 0.67 m, 0.49 m, and 0.64 m, respectively. Simulated PS values were also overestimated at 1.59 m, 1.61 m, and 1.0 m, compared to the recorded surge elevations of 1.17 m, 0.72 m, and 0.52 m at IC, KO, and MP, respectively.

Numerical tests were also conducted for Typhoon Bolaven, and the results were analyzed for the three main tidal stations. According to the recorded data, the FSs occurred at least 12 h ahead of the typhoon passing through the same latitudes nearby the stations. The recorded primary SHs were 0.66 m, 1.19 m, and 1.52 m, while simulated values were 0.61 m, 0.64 m, and 1.07 m for the MP, KO, and IC stations, respectively. The lowest discrepancy in the numerically simulated results was for the KO station at 46%. However, this tendency was different for the FSs. The observed FS values were 0.38 m, 0.61 m, and 0.47 m, while calculated values were 0.31 m, 0.42 m, and 0.49 m for the MP, KO, and IC stations, respectively. The simulated and observed FS values were similar, but with less discrepancy observed when compared to the PS values.

Through these tests for momentum terms, we found that the most influential factor for SH was surface stress due to strong vortex wind. Simulations that neglected wind resulted in an FS reduced by a maximum of 82% at IC and a minimum of 76% at KO for Typhoon Prapiroon. The maximum SH was reduced by 63% at MP, and up to 82% in IC (Table 4). In simulating Typhoon Bolaven, the reduced change in FS height was 98% at IC and 81% at MP when winds were neglected. The maximum SH was reduced by at least 45% at KO, and up to 74% at IC under these conditions.

When the central pressure was ignored, the maximum sea level induced by Typhoon Bolaven was reduced by 29–38%. In simulating Typhoon Prapiroon, the maximum SH was reduced by 52–72%, and the FS height changed by 45–78% (Table 4).

4.4. Sensitivity analysis for typhoon characteristics

As wind forcing acts as the major factor affecting the FS and PS, we conducted further sensitivity tests for vortex movement. We modified the size of the wind field (i.e., the maximum radii of vortex corresponding to 34 kt, R_{max}), and the maximum sustained wind speed V_{max} by ± 20% compared to the best track data.

Through the simulated results (Fig. 9, Table 5), we found that the size of wind field, R_{max}, was a key factor in determining FS heights, resulting in a 67–79% increase in height for a 20% larger storm size,

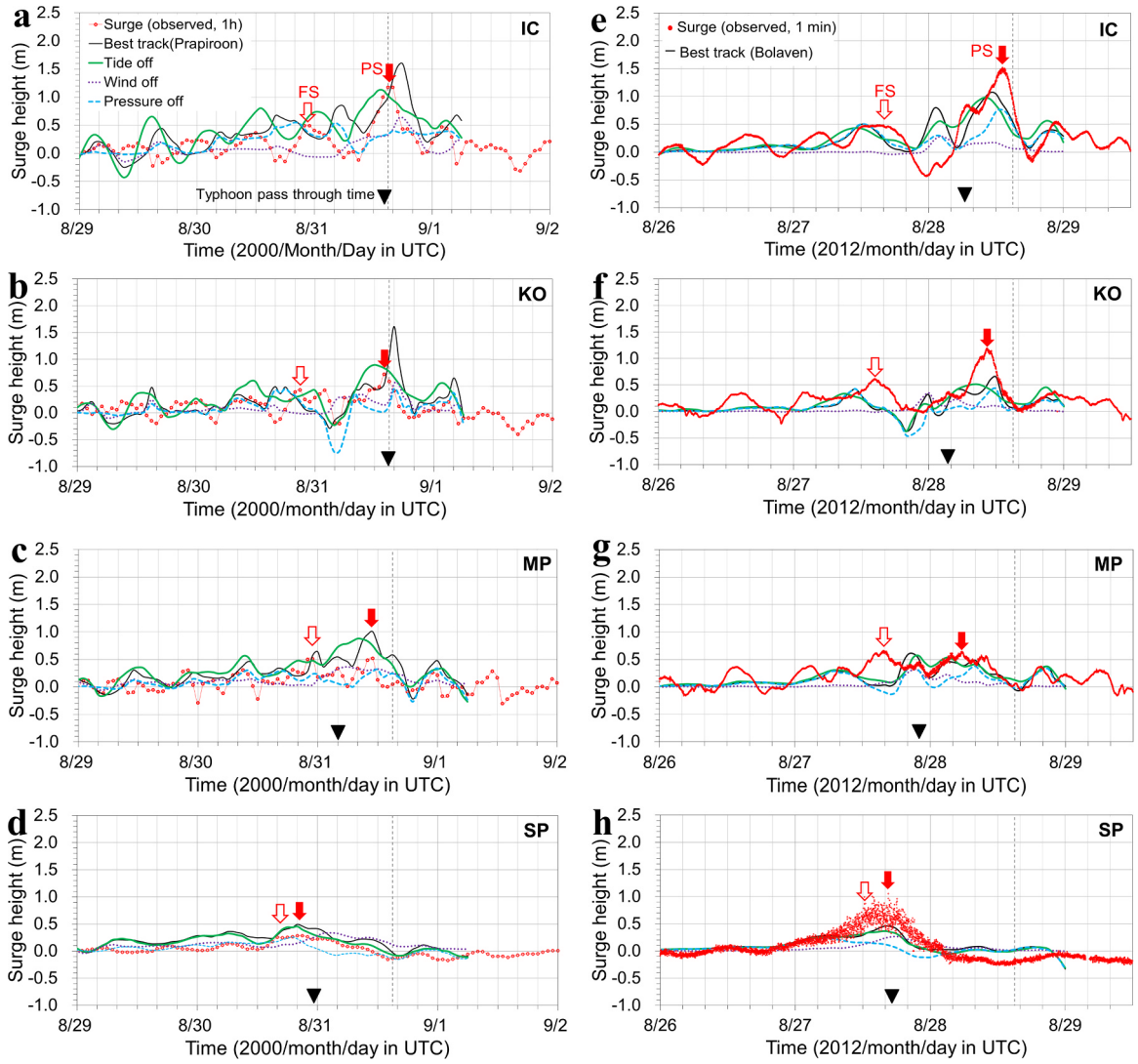

Fig. 8. Momentum forcing effect on SHs for Typhoons Prapiroon (left panel) and Bolaven (right panel).

and a 53–64% decrease in height for a 20% decrease in storm size when compared to the recorded FS elevation at IC and KO, respectively. Slow-moving typhoons could only increase the surge elevation by 6–19%, and faster typhoons decreased FS heights by 2–14% at IC and KO.

The maximum velocity for FSs was not consistent. Through sensitivity tests, we determined that when large storms move slowly, greater increases in FS height may occur. These results are consistent with the high FS (2 m) of Hurricane Ike. The vortex size of Hurricane Ike was 74 km at −7 h landfall. The mean forward speed of Hurricane Ike was 17 km h^{-1} in the GOM; for comparison, the speeds of Hurricanes Rita, Katrina, Gustav, and Ivan were 18 km h^{-1}, 20 km h^{-1}, 27 km h^{-1}, and 27 km h^{-1}, respectively according to the ATCF.

In addition to wind field parameter sensitivity analyses, we tested two typical wind vortex forms; the symmetrical formulation suggested by Holland (1980), and the dynamic asymmetric representation of Mattocks and Forbes (2008), to qualitatively determine wind field differences. Moreover, data from the Regional Data Assimilation and Prediction System (RDAPS) of the KMA were extracted at every sixth hour on the regular grid of 0.11 × 0.11 degrees for the Asia Pacific region, and used to compare parametric wind models. The simulated results are shown in Fig. 10.

Through these simulations, we found that storm surge responses were mainly dependent upon vortex shape, regardless of the location of vortex eye and landfall. However, when approaching the landfall location (in this case, from MP to KO, and then to IC) the FS and PS increased but exhibited some deviation according to the vortex formulation. Numerical tests revealed that the pressure depression of storms directly affected PSs, but the magnitudes were not sensitive to surface wind stress at all stations. Hence, storm vortex representation, such as the appropriate asymmetric shape showing local intensity, was found to be the major factor for sea surface alteration for both the PS and FS. Contrary to expectations, the best simulation result was achieved by specifying wind velocities and pressures on a regular structured grid (i.e., specifying NWS as option 6 option in the ADCIRC based on meteorological data from the RDAPS of the KMA), as shown in Table 5.

4.5. Grid refinement test

In this study, the effects of grid refinement on SHs were also analyzed by applying three grid structures, NWP-G57k, G116k, and G258k (Suh et al., 2015). Based on the numerical tests, grid resolutions, particularly around coastal areas, slightly affected both SH and the appearance time at most tidal stations. Grid refinement could not guarantee low error values, but a moderate resolution, such as G57k and G116k, with finer resolutions around shallow coastal areas, provided reasonable results. Regarding station IC, the coarse grid, G57k, surprisingly yielded better results than the finer grids (Fig. 11). Since IC is located within a concave coastal geometry, similar to Galveston Bay of the LATEX, it may not be affected by grid refinement.

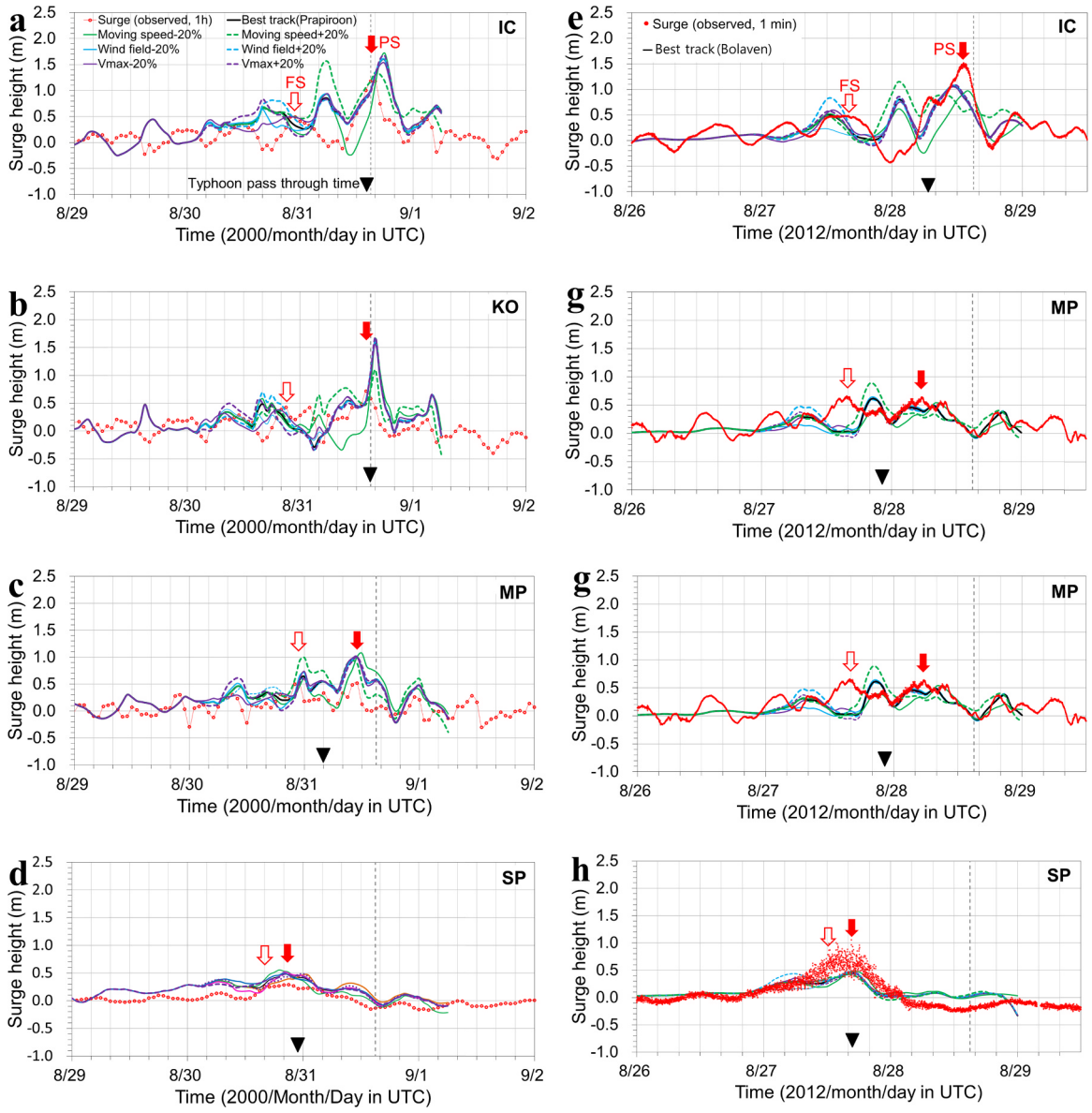

Fig. 9. Comparisons of PS and FS for the four recording stations along the WCK (black dashed line: landfall time, black arrowhead: pass through time) based on sensitivity tests of Typhoons Prapiroon (left panel) and Bolaven (right panel).

5. Discussion

One of the factors affecting FS formation is the geostrophic effect in the form of the Ekman setup due to the Coriolis force (Hope et al., 2013; Kerr et al., 2013a, 2013b). Rego and Li (2010) indicated that the alongshore component of wind stress may cause a storm surge if the coast is to the right of the wind in the northern hemisphere, and that the across-shore component of wind stress becomes more important as water depth decreases. Higher water levels occur in coastal areas to the right of a storm track in the northern hemisphere.

Observed sea levels at the tide gauging stations described in Section 2 and those simulated at the comparison stations described in Section 4.2 on the WCK displayed the presence of a coastally trapped Kelvin waves. Kelvin waves were also present in other major storm surge events. A Kelvin wave progressed westward as a surge associated with the strong atmospheric forcing of Hurricane Frederic in 1992 as it crossed the eastern GOM (D'Sa et al., 2011), and this was also observed for Hurricane Ivan in 2004 (Zamudio and Hogan, 2008). The FS associated with a Kelvin wave is characterized by the relationship between geophysical resonance and the storm movement speed. When Hurricane Ike approached the LATEX coast, the movement speed was estimated at 17 m s^{-1} (D'Sa et al., 2011), which matches the wave speed of a coastally trapped free Kelvin wave of $\sqrt{gh}$ assuming mean water depth of 30 m along 28.5° N latitude.

Storm surges may be related to resonance, wherein a disturbance traveling parallel to the coast over a linearly sloping bottom may lead to forced ocean wave amplification (Thiebaut and Vennell, 2011). Thiebaut and Vennell (2011) demonstrated that resonance occurs when the alongshore phase speed of a forced wave matches the free Kelvin-wave phase speed. They revealed that a sub-critical resonance occurs when a relatively slow moving forced wave in a flat-bottomed ocean crosses a vertical coast at a particular angle (i.e., an inclined angle of ~15° in the case of Hurricane Katrina), which may enhance coastal surges under sub-critical storms.

5.1. Coastally trapped wave characteristics based on historical typhoon surges

Understanding the propagation patterns of storm surges in terms of Kelvin waves in the YS is important in FS analysis. To determine the distinct characteristics of coastally trapped waves induced by tropical storm surges, additional four typhoon tracks were considered. To capture the distinctive tropical storm surge characteristics for landfalling

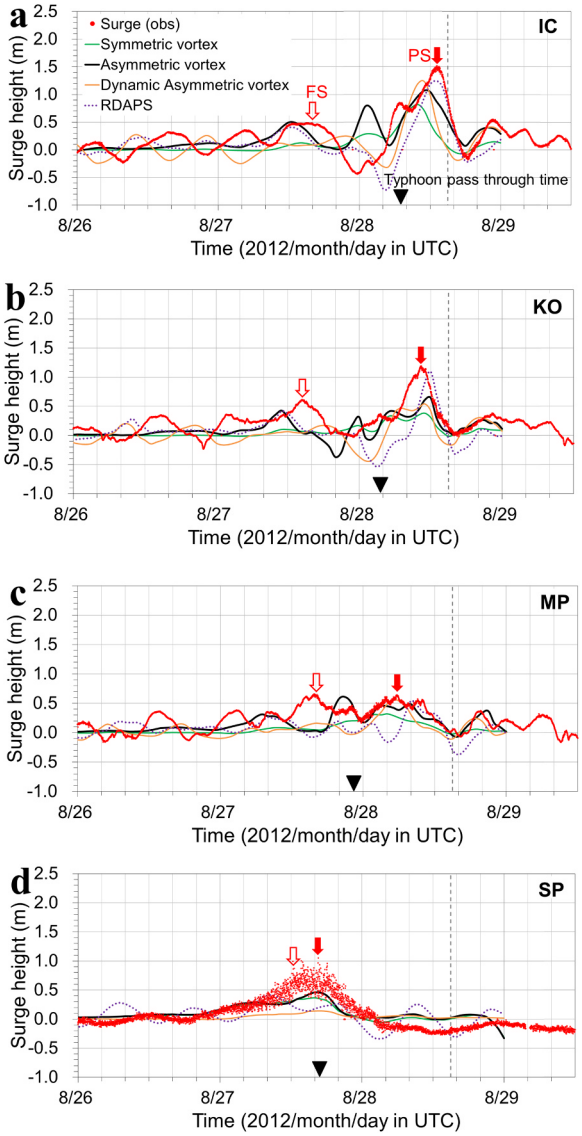

Fig. 10. Comparisons of PS and FS for Typhoon Bolaven after applying different vortex shapes (black dashed line: landfall time, black arrowhead: pass through time).

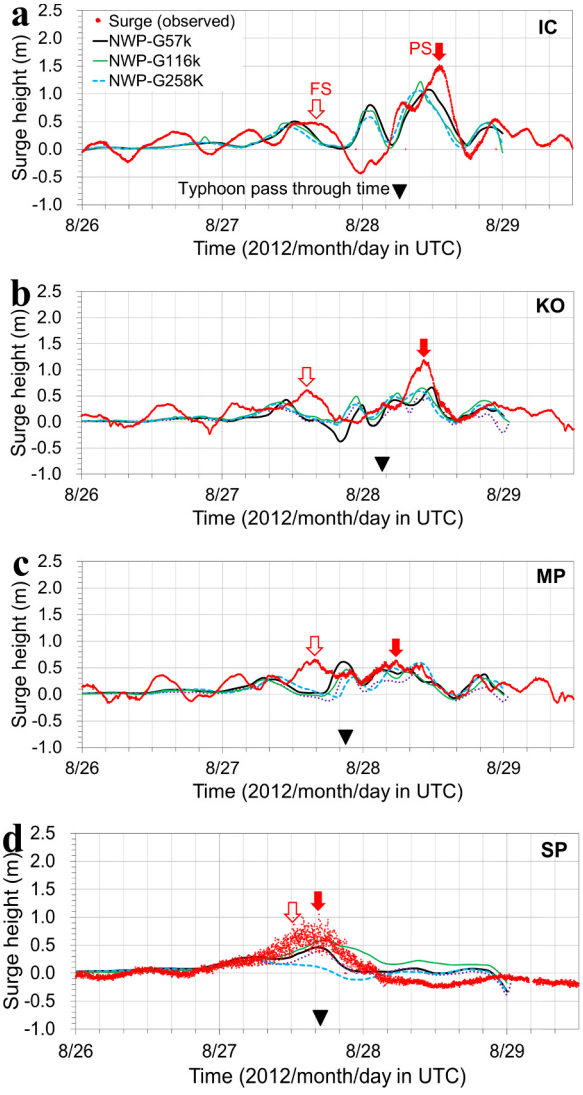

Fig. 11. Surge elevations depending on grid refinement.

or coast tracking typhoons Kompasu, Ewiniar, Muifa, and Winnie were analyzed with respect to IC station considering the unique curvature of the WCK (Fig. 12). These typhoons were selected among the historical tracks to compare with Bolaven and Prapiroon.

The observed water surface anomalies associated with the passing (landfall) of typhoons, exhibit a clear pattern in which FS are present (absent) as shown in upper (lower) panel of Fig. 13. For Typhoon Winnie, which made landfall in China, FS occurred at IC with 0.6 m induced by the resonance of the YS (Moon et al., 2003); the magnitude of PS was approximately the same as FS. In the case of Typhoon Muifa, the combined effects of tides and surges caused rather complex FS appearances owing to coastal tracking with wider D_s than FS characteristics when compared to Typhoons Bolaven and Prapiroon (Fig. 3). However, with a short D_s, landfall cases, such as Typhoons Ewiniar and Kompasu, exhibited no clear FS. Thus, both sufficient D_s and radius of maximum wind (RMW), as well as slow coastal tracking of typhoons are key factors in the generation of FS.

5.2. Comparison of forerunner surge responses in the Yellow Sea (YS) and Gulf of Mexico (GOM)

The combined effects of the geostrophic balancing force, storm size,

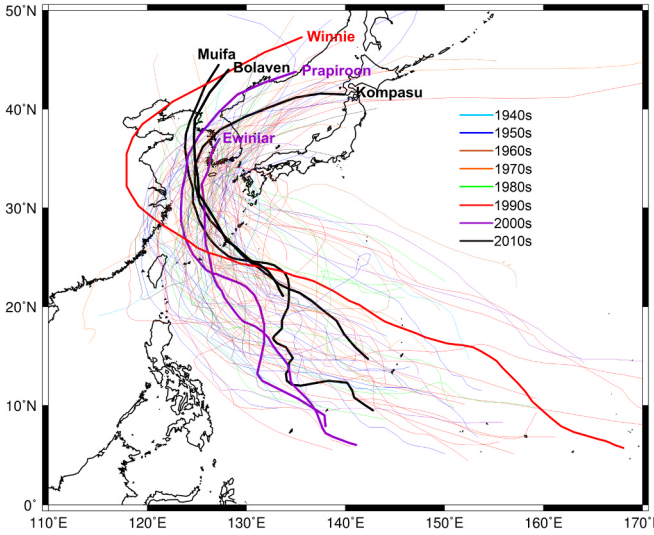

Fig. 12. Selected six typhoon tracks showing coastal tracking or landfall with respect to the IC station of the WCK.

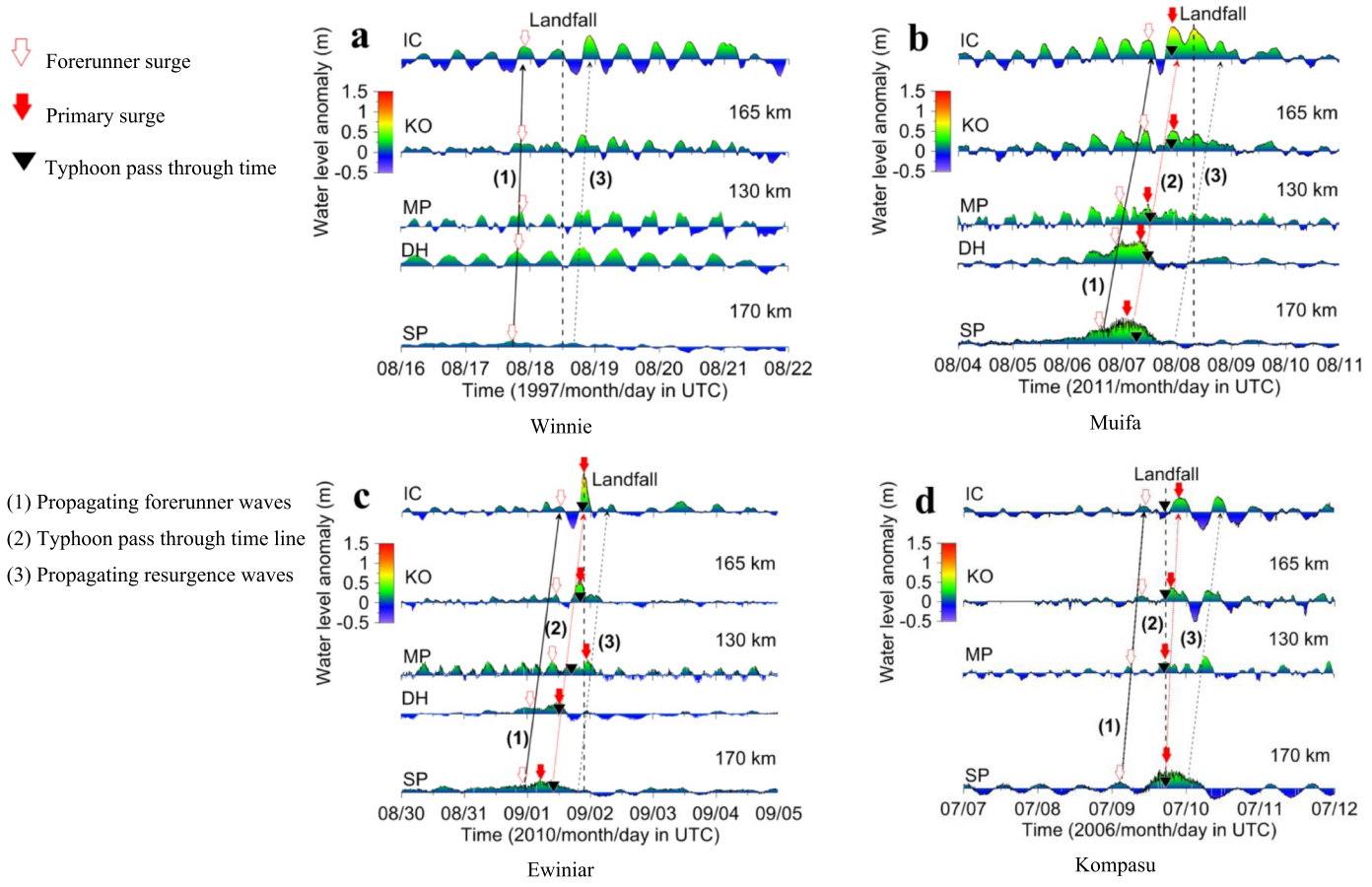

Fig. 13. Water surface anomalies corresponding typhoons passing (landfall) to the IC stations in upper (lower) panel.

movement speed, geostrophic parameters, and detached distance of track routes can result in FS and PS. When typhoons or hurricanes are moving toward continental shelves, different forces come into play to maintain balance. During this period, some forces exhibit less influence, while geostrophic balance plays a major role in certain areas. To determine regional characteristics, we compared Hurricanes Rita and Ike in the GOM with Typhoons Prapiroon and Bolaven in the YS. Because the WCK in the YS lies on the inner shelf, the effects and driving forces of storm surges may differ from those of the LATEX coast of the GOM. In particular, storm surges are strongly influenced by the geometry of the basin and continental shelf leading up to the coastal floodplain (Resio and Westerink, 2008), thus performing comparison between the two basins may provide insight into the relative influence of different driving forces with respect to coastal geometry. Surges due to onshore winds may typically be maximized at a distance 1–3 times the RMW in the GOM (Resio et al., 2009); meanwhile, the onshore effects of effective surge fetch may not be important in the WCK because of the inner shelf environment of the YS. As both basins are located in the northern hemisphere, coasts on the right side are affected by the Ekman and Kelvin wave setup. When a typhoon track moves into the YS, the FS could occur along the WCK. However, the mean depth of the YS is only 44 m, which is not comparable with the GOM (1500 m) (Hope et al., 2013; Kerr et al., 2013a, 2013b).

There are distinct differences between onshore setup processes developed through wind stress on the inner shelf for the YS, where bottom friction plays an important role due to the shallow depth, and the mid-outer shelf (GOM; Lentz and Fewings, 2012). Thus, FS in the WCK and the GOM should be treated differently. Though geostrophic flow on the inner shelf may not be dominant, the simple assumption can be helpful for comparing FS between the YS and the GOM.

The FS is likely to increase if a cyclone moves slowly over the Ryukyu Islands onto the continental shelf of the YS, or along the continental shelf in the GOM. The Coriolis force has a substantial effect on the FS in the GOM (Hope et al., 2013; Kennedy et al., 2011). However, this is not applicable in the WCK, owing to its shallow depth. The wind setup resulting from the surface stress has a greater influence in this shallow and macro-tidal environment.

We found that the slower typhoons passing over the Ryukyu Islands and entering the continental shelf yielded the higher FS heights. The recorded FS heights at the IC station were 0.5 m for Typhoons Prapiroon, Muifa, and Bolaven, and 0.2 and 0.25 m for Typhoons Ewiniar and Kompasu, respectively. The translation speeds were 7 km h^{-1} in Typhoon Prapiroon, 12 km h^{-1} in Typhoon Muifa, 19 km h^{-1} in Typhoon Bolaven, 20 km h^{-1} in Typhoon Ewiniar, and 26 km h^{-1} in Typhoon Kompasu. Recorded FS heights in the GOM induced by slowly moving Hurricanes Ike (17 km h^{-1}), Rita (18 km h^{-1}), Katrina (20 km h^{-1}), Gustav (27 km h^{-1}), and Ivan (27 km h^{-1}) over the continental shelf yielded relatively higher FS heights similarly to FS in the YS. This suggests the possibility of real-time FS forecasting if a typhoon early warning system (EWS) on the WCK is employed by tracing the track and moving speed onto the continental shelf. This can also be applied to the GOM, considering that the moving speed is relatively slow compared to historical hurricanes.

Kennedy et al. (2011) pointed that continental shelf waves were the primary reason for the formation of the forerunner of Hurricane Ike. They identified the waves as sub-inertial and barotropic continental shelf waves. A moving storm crossing a shelf break can generate resonance even if its incident angle does not precisely meet the resonant conditions. However, the transient amplification will be stronger for a disturbance with an incident angle at or near the critical angle. Therefore, storms crossing the shelf with inclined angles, such as 15°, as in the case of Hurricane Katrina, can possibly cause greater surges, and are more likely to retain higher edge wave energies within the shelf

after the passage of the storm (Thiebaut and Vennell, 2011). Suh et al. (2015) also suggested that FS could be generated when storms were crossing the Ryukyu Islands from the NWP region to the YS, and moving toward the WCK. According to their findings, the FS occurs as a result of the geostrophic effect, and it may be considered a type of sub-critical resonance. As historical data for storm surges are limited, it is difficult to determine a critical entering angle. Nevertheless, all five typhoons producing FS that we investigated entered at angles < 20°. Synthetic storms may be employed to investigate the critical entering angle precisely in future work.

5.3. Nonlinear effects on tide-surge interactions in forerunner surges

To determine the positive or negative impacts of ambient strong tidal flows on SHs in macro-tidal environments, we performed simulations shifting the tidal movement by 3–6 h faster or slower to account for traveling tidal currents. As the WCK has a macro-tidal environment, the ambient, strong tidal fluctuations directly affect SH due to nonlinear interactions with tidal currents and Kelvin-type geostrophic flows. In addition, tidal asymmetry, flood dominance along the WCK (Suh et al., 2014), especially at KO to IC stations, and influenced by the nonlinear

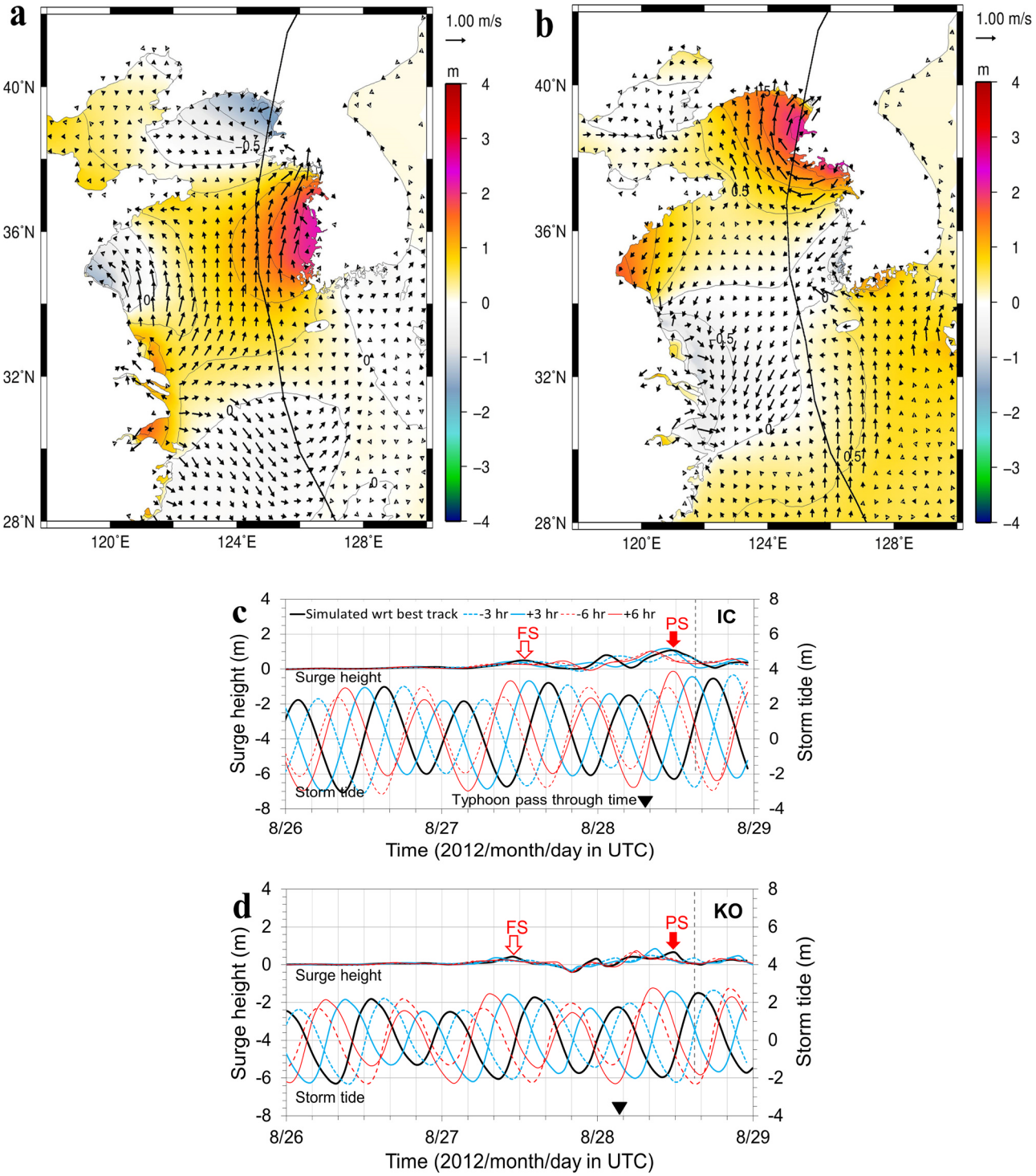

Fig. 14. Comparison of FS/PS variations for Typhoon Bolaven with respect to tidal environment: (a) flood current - 271400Z, (b) ebb current - 271900Z (vector: current, contour: storm tide), (c) Incheon and (d) Kunsan outer port.

interactions between tides and Kelvin waves during typhoon tracking along the coast, should be precisely investigated. To determine the effects of nonlinear interactions on FS, we adjusted the peak surge time by moving the typhoon earlier or later to meet the strongest flood condition (i.e., to simulate flows at the time of surge occurrence coinciding with the maximum northward flood states).

Results revealed that a historical FS at IC due to Typhoon Bolaven had a height of 0.49 m during the flooding flow. However, by delaying the landfall of the typhoon by 6 h to coincide with the ebb condition, the FS decreased by 43% and had a height of 0.28 m. The maximum PS height at flood flow was 1.07 m, while it was 0.51 m when the typhoon appeared 6 h later coinciding with the ebb flow. The nonlinear effects of tide-surge interactions are important in shallow water areas with a large tidal range (Wolf, 2009). Prandle and Wolf (1978), Wolf (1981), Davies and Lawrence (1994), Jones and Davies (1998), and Horsburgh and Wilson (2007) described the effects of tide-surge interactions. The tidal phase is advanced due to the deeper water caused by the presence of a positive surge level. The difference between the phase-shifted and undisturbed tide is added to the surge to yield the net tidal residual, which has a peak of 3 h before the predicted high water, as shown in Fig. 14.

Rego and Li (2010) computed the nonlinear interaction term in surge simulations and found that a negative interaction term was calculated near the peak surge. Nonlinearity decreased the peak storm tide. To confirm if this pattern was maintained under a different tide, the same wind forcing was used with landfall occurring at low tide and a doubled tidal amplitude. The same pattern occurred for the nonlinear effect: the nonlinear term opposed the tide by enhancing storm tide heights when the tide was near its minimum. Their study showed that the locations of landfall would experience nonlinearities opposing the tide, reducing storm tide heights when the tide was in the rising stage. These locations would experience nonlinearities enhancing the storm tide during ebbing or near low tide. For low- or high-tide landfalls, nonlinearity effects were constructive and destructive to total storm tide, respectively. Moreover, they demonstrated that the semidiurnal tide had larger nonlinear effects compared to the diurnal tide over a wide shelf due to amplification of nonlinearity. According to the simulated results in this study, almost this exact situation is observed along the WCK when typhoons enter the continental shelf of the YS and make landfall on the northern part of the Korean Peninsula as occurred with both Typhoons Bolaven and Prapiroon.

5.4. Limitations of track information in storm surge prediction

Even when the best track data were used for reconstruction or verification purposes in the storm surge modeling, the calculated result of the storm surge differed from the actual observations due to uncertainties in the best track data itself. Consequently, the simulation results using best track data in this study do not match well with the surge elevation (Figs. 8 and 9). Torn and Snyder (2012) and Cha et al. (2016) addressed the uncertainties in the central location, central pressure, and maximum wind speed in best tracks. Cha et al. (2016) suggested a best track analysis technique to minimize the uncertainty of the typhoon forecast data. Zhong et al. (2010) proposed a method to improve storm surge prediction using ensemble meteorological forecasts. In addition, Forbes et al. (2014) presented improved results considering the precise grid structure, asymmetric wind field, and tidal coupling to improve the results of a parameterized model. However, errors in the parameter model and best track data still failed to produce satisfactory results. One of the possible reasons of inaccuracies in surge modeling is the use of the un-calibrated constant vortex shape parameter of Holland. Resio et al. (2009, 2017) addressed surge responses dependent upon this parameter, and verified that some values falling into even a fairly small range of 0.9–1.6 in mature storms within the GOM would enhance surge simulation. Another cause of inaccuracy in storm surge modeling may result from uncertain bottom friction application and grid resolution (Veeramony et al., 2012). However, as discussed by Suh et al. (2015), it has been determined that even with best track data, improvement in the accuracy of the storm surge height is limited by grid refinement.

In the simulations, though best track data were adopted, it was difficult to obtain a satisfactory fit between observed and modeled water surface anomalies, especially in terms of peak timing. The reason for this may be the combination of deficiencies in the numerical models, meteorological forcing, and analyzing techniques. In addition, uncertainties in the input forcing data could not be removed. Thus, more accurate cyclone information is still required. Because it is difficult to implement exact meteorological forcing in a surge model, more reliable representation of cyclones should be provided in further studies to enhance the reliability of FS and PS forecasting. In the case of EWS operation, if information on the cyclone track, movement speed, and angle of entry into the continental shelf can be obtained in real-time, accurate forecasts of FSs can be achieved.

6. Conclusions

In this study, FSs and PSs induced by typhoons were investigated through the analysis of both observation and numerical simulation results to understand the effects of geostrophic balance on storm surges. In particular, we attempted to determine the mechanism underlying FS formation during the entrance of typhoons onto the continental shelf of the ECS to the YS when crossing over the Ryukyu Islands. Geophysical aspects, including coastally trapped Kelvin waves and the geostrophic setup effect, were considered.

Sensitivity tests were performed to identify the most important factors affecting the formation of FSs. In the sensitivity tests, the depth-dependent bottom friction coefficient, typhoon moving speed, size of the wind field, V_{max} and R_{max}, and tidal forcing terms in the momentum equations were analyzed. According to the overall sensitivity tests, higher FSs formed when large storms moved slowly. Furthermore, the Coriolis force does not influence FS under shallow depth conditions in the YS, where the Coriolis term is smaller than the other terms over the inner shelf; on average, onshore of the 20-m isobath, the term is less than half as large as the along-shelf wind stress term (Lentz and Fewings, 2012). However, the Coriolis force seemed to play an important role in both FS and PS generation in deeper conditions in the GOM.

The importance of the nonlinear interaction term in surge simulations was assessed by forcing the high and low tide to coincide with the storm tide. For low-tide landfalls, nonlinear effects were constructive to total storm tide; meanwhile, for high-tide landfalls, their effects were destructive to total storm tide. The results show that the nonlinear effects of tide-surge interactions are important in shallow water areas with large tidal ranges (Wolf, 2009). Grid refinement tests were also conducted. Low error rates could not be guaranteed with finer grid structures, so a moderate resolution grid with a finer resolution in the shallow coastal areas was considered acceptable. However, even adopting the best tracks in the simulation with the most suitable grid structure, simulation accuracy of the storm surge height and timing was limited. Because the combination of reasons leading to mismatches in peak timing were not well-resolved in this study due to deficiencies in the numerical models, meteorological forcing, and analyzing techniques, continued study aimed at not only increasing the accuracy of storm surges simulations, but also representing the appropriate characteristics of storm vortices in coupled tide-surge models is needed.

Comparative analyses were conducted to determine the effects of geometry and separation distance on the formation of FSs. Numerical Results showed that a sub-critical resonance could occur when slow-moving typhoons move from the NWP to the continental shelf of the ECS and YS by crossing over the Ryukyu Islands. In addition, through the comparison of recorded historical data between the YS and the GOM, we found that slow-moving cyclones crossing over continental

shelves at speeds less than 20 km h^{-1}, which can be thought of as a threshold moving speed for FS generation, yielded relatively higher FS heights. Hence, waves obliquely crossing over the shelf slope at particular angles within 20° to the normal direction should be carefully monitored and considered in EWS or near real-time forecasting of storm surges as this phenomenon could be a major factor for the formation of FS in terms of free Kelvin wave propagation.

Through this study, we have determined that the mechanism of forerunner propagation along the WCK as Kelvin wave propagation. The results of this study may be useful for enhancing FS prediction during typhoon or hurricane seasons, and thus in providing early warnings to prevent disasters.

Acknowledgments

We greatly appreciate the insightful comments and suggestions by the three anonymous reviewers. We also thank Dr. William Pringle from the Computational Hydraulics Lab of Notre Dame University for valuable comments and discussion. This work was supported by the National Research Foundation of Korea (NRF) grant funded by the Korea government, MSIP (No. NRF-2017R1A2B4008613).

References

Amante, C., Eakins, B.W., 2009. ETOPO1 1 Arc-minute global relief model: procedures, data sources and analysis. National Geophysical Data Center Marine Geology and Geophysics Division Boulder, Colorado. https://doi.org/10.7289/V5C8276M. (NOAA Technical Memorandum NESDIS NGDC-24).

Bell, C., Vassie, J.M., Woodworth, P.L., 1999. POL/PSMSL tidal analysis software kit 2000(TASK-2000). CCMS Proudman Oceanographic Laboratory, Bidston Observatory, Birkenhead, Merseyside (20 pp) (Permanent Service for Mean Sea Level).

Bertin, X., Bruneau, N., Breilh, J.F., Fortunato, A.B., Karpytchev, M., 2012. Importance wave age and resonance in storm surge: the case Xynthia, Bay of Biscay. Ocean Model. 42, 16–30. https://doi.org/10.1016/j.ocemod.2011.11.001.

Blanton, B., McGee, J., Fleming, J., Kaiser, C., Kaiser, H., Lander, H., Luettich, R.A., Dresback, K., Kolar, R., 2012. Urgent computing of storm surge for North Carolina's coast. Proc. Comput. Sci. 9, 1677–1686. https://doi.org/10.1016/j.procs.2012.04.185.

Carrère, L., Lyard, F., Cancet, M., Guillot, A., Roblou, L., 2012. FES2012: A new global tidal model taking advantage of nearly twenty years of altimetry, Proceeding of the 20 Years of Progress in Radar Altimetry Symposium, Venice, Italy.

Cha, Y., Kim, J., Kang, K., Kang, N.Y., Yun, W.T., 2016. A study on the determination of Korea affecting tropical cyclone center for best tracking. Adv. Meteor. 2016, 1–13. https://doi.org/10.1155/2016/5946342.

Davies, A.M., Lawrence, J., 1994. The response of the Irish Sea to boundary and wind forcing: results from a three-dimensional hydrodynamic model. J. Geophys. Res. **99**. https://doi.org/10.1029/94JC01568.

Dietrich, J.C., Zijlema, M., Westerink, J.J., Holthuijsen, L.H., Dawson, C., Luettich, R.A., Jensen, R.E., Smith, J.M., Stelling, G.S., Stone, G.W., 2011. Modeling hurricane waves and storm surge using integrally-coupled, scalable computations. Coast. Eng. 58 (1), 45–65. https://doi.org/10.1016/j.coastaleng.2010.08.001.

D'Sa, E.J., Korobkin, M., Ko, D.S., 2011. Effects of Hurricane Ike on the Louisiana–Texas coast from satellite and model data. Remote Sens. Lett. 2 (1), 11–19. https://doi.org/10.1080/01431161.2010.489057.

Forbes, C., Rhome, J., Mattocks, C., Taylor, A., 2014. Predicting the storm surge threat of hurricane sandy with the national weather service SLOSH model. J. Mar. Eng. 2 (2), 437–476. https://doi.org/10.3390/jmse2020437.

Hoffman, R.N., Dailey, P., Hopsch, S., Ponte, R.M., Quinn, K., Hill, E.M., Zachry, B., 2010. An estimate of increases in storm surge risk to property form sea level rise in the first half of the twenty-first century. Weather Clim. Soc. 2, 271–293.

Holland, G.J., 1980. An analytical model of the wind and pressure profiles in hurricanes. Mon. Weather Rev. 108, 1212–1218. https://doi.org/10.1175/1520-0493(1980)108<1212:AAMOTW>2.0.CO;2.

Hope, M.E., Westerink, J.J., Kennedy, A.B., Kerr, P.C., Dietrich, J.C., Dawson, C., Bender, C.J., Smith, J.M., Jensen, R.E., Zijlema, M., Holthuijsen, L.H., Luettich, R.A., Powell, M.D., Cardone, V.J., Cox, A.T., Pourtaheri, H., Roberts, H.J., Atkinson, J.H., Tanaka, S., Westerink, H.J., Westerink, L.G., 2013. Hindcast and validation of hurricane Ike (2008) waves, forerunner, and storm surge. J. Geophys. Res.: Oceans 118, 4424–4460. https://doi.org/10.1002/jgrc.20314.

Horsburgh, K.J., Wilson, C., 2007. Tide-surge interaction and its role in the distribution of surge residuals in the North Sea. J. Geophys. Res. 112. https://doi.org/10.1029/2006JC004033.

IPCC, 2011. Summary for Policymakers. Intergovernmental Panel on Climate Change Special Report on Managing the Risks of Extreme Events and Disasters to Advance Climate Change Adaptation. Cambridge University Press, Cambridge, United Kingdom and New York, NY, USA.

Jones, J.E., Davies, A.M., 1998. Storm surge computations for the Irish Sea using a three-dimensional numerical model. Cont. Shelf Res. 18 (2), 201–251. https://doi.org/10.1016/S0278-4343(97)00062-9.

Kennedy, A.B., Gravois, U., Zachry, B.C., Westerink, J.J., Hope, M.E., Dietrich, J.C., Powell, M.D., Cox, A.T., Luettich, R.A., Dean, R.G., 2011. Origin of the hurricane Ike forerunner surge. Geophys. Res. Lett. 38. https://doi.org/10.1029/2011GL047090.

Kerr, P.C., Donahue, A.S., Westerink, J.J., Luettich, R.A., Zheng, L.Y., Weisberg, R.H., Huang, Y., Wang, H.V., Teng, Y., Forrest, D.R., Roland, A., Haase, A.T., Kramer, A.W., Taylor, A.A., Rhome, J.R., Feyen, J.C., Signell, R.P., Hanson, J.L., Hope, M.E., Estes, R.M., Dominguez, R.A., Dunbar, R.P., Semeraro, L.N., Westerink, H.J., Kennedy, A.B., Smith, J.M., Powell, M.D., Cardone, V.J., Cox, A.T., 2013a. U.S. IOOS coastal and ocean modeling testbed: inter-model evaluation of tides, waves, and hurricane surge in the Gulf of Mexico. J. Geophys. Res. Ocean 118 (10), 5129–5172. https://doi.org/10.1002/jgrc.20376.

Kerr, P.C., Martyr, R.C., Donahue, A.S., Hope, M.E., Westerink, J.J., Luettich, R.A., Kennedy, A.B., Dietrich, J.C., Dawson, C., Westerink, H.J., 2013b. U.S. IOOS coastal and ocean modeling testbed: evaluation of tide, wave, and hurricane surge response sensitivities to mesh resolution and friction in the Gulf of Mexico. J. Geophys. Res.: Oceans 118 (9), 4633–4661. https://doi.org/10.1002/jgrc.20305.

Kim, C.S., Lim, H.S., Jeong, J.Y., Shim, J.S., Moon, I.J., Oh, Y.J., You, J.Y., 2014. Responses of coastal waters in the Yellow Sea to Typhoon Bolaven. J. Coast. Res. 70, 278–283.

Kim, H.J., Suh, S.W., 2016. Probabilistic coastal storm surge analyses using synthesized tracks based on historical typhoon parameters. J. Coast. Res. 75, 1132–1136. https://doi.org/10.2112/SI75-227.1.

Lentz, S.J., Fewings, M.R., 2012. The wind- and wave-driven inner-shelf circulation. Annu. Rev. Mar. Sci. 4, 317–343.

Luettich, R.A., Westerink, J.J., Scheffner, N.W., 1992. ADCIRC: an advanced three-dimensional circulation model for shelves coasts and estuaries report 1: Theory and methodology of ADCIRC-2DDI and ADCIRC-3DL. Dredging Research Program Technical Report DRP-92-6, US Army Corps of Engineers Waterways Experiment Station, Vicksburg. 137 pp.

Mattocks, C., Forbes, C., 2008. A real-time, event-triggered storm surge forecasting system for the state of North Carolina. Ocean Model. 25, 95–119. https://doi.org/10.1016/j.ocemod.2008.06.008.

Moon, I.J., Oh, I.S., Murphy, T., Youn, Y.H., 2003. Causes of the unusual coastal flooding generated by typhoon Winnie on the West Coast of Korea. Nat. Hazard 29, 485–500.

Prandle, D., Wolf, J., 1978. The interaction of surge and tide in the North Sea and River Thames. Geophys. J. R. Astron. Soc. 55, 203–216. https://doi.org/10.1111/j.1365-246X.1978.tb04758.x.

Rego, J.L., Li, C., 2010. Nonlinear terms in storm surge predictions: effect of tide and shelf geometry with case study from hurricane Rita. J. Geophys. Res. 115, C06020. https://doi.org/10.1029/2009JC005285.

Resio, D.T., Westerink, J.J., 2008. Modeling the physics of storm surges. Phys. Today. https://doi.org/10.1063/1.2982120.

Resio, D.T., Irish, J., Cialone, M.A., 2009. A surge response function approach to coastal hazard assessment –part 1: basic concepts. Nat. Hazards 51, 163–182. https://doi.org/10.1007/s11069-009-9379-y.

Resio, D.T., Powell, N.J., Cialine, M.A., Das, H.S., Westerink, J.J., 2017. Quantifying impacts of forecast uncertainties on predicted storm surges. Nat. Hazards 88, 1423–1449. https://doi.org/10.1007/s11069-017-2924-1.

Sebastian, A., Proft, J., Dietrich, J.C., Du, W., Bedient, P.B., Dawson, C.N., 2014. Characterizing hurricane storm surge behavior in Galveston Bay using the SWAN + ADCIRC model. Coast. Eng. 88, 171–181. https://doi.org/10.1016/j.coastaleng.2014.03.002.

Sudre, J., Maes, C., Garcon, V., 2013. On the global estimates of geostrophic and Ekman surface currents. Limnol. Oceanogr. Fluids Environ. 3, 1–20. https://doi.org/10.1215/21573689-2071927.

Suh, S.W., Lee, H.Y., Kim, H.J., 2014. Spatio-temporal variability of tidal asymmetry due to multiple coastal constructions along the west coast of Korea. Estuar. Coast. Shelf Sci. 151, 336–346. https://doi.org/10.1016/j.ecss.2014.09.007.

Suh, S.W., Lee, H.Y., Kim, H.J., Fleming, J.G., 2015. An efficient early warning system for typhoon storm surge based on time-varying advisories by coupled ADCIRC and SWAN. Ocean Dyn. 65 (5), 617–646. https://doi.org/10.1007/s10236-015-0820-3.

Thiebaut, S., Vennell, R., 2011. Resonance of long waves generated by storms obliquely crossing shelf topography in a rotating ocean. J. Fluid Mech. 682, 261–288. https://doi.org/10.1017/jfm.2011.221.

Torn, R.D., Snyder, C., 2012. Uncertainty of tropical cyclone best-track information. Weather Forecast. 27, 715–729. https://doi.org/10.1175/WAF-D-11-00085.1.

Veeramony, J., Condon, A., Hebert, D., 2012. Effect of coupling wave and flow dynamics on hurricane surge and inundation. Pro. twenty-second ISOPE, Rhodes, Greece, pp. 1503–1507.

Wang, B., 2002. Kelvin waves. In: Shankar, M. (Ed.), Encyclopedia of Atmospheric Sciences. Elsevier, Amsterdam, pp. 1062–1068.

Weaver, R.J., Slinn, D.N., 2004. Effect of wave forcing on storm surge. Proceedings of the 29th International Conference on Coastal Engineering, pp. 1532–1538.

Wessel, P., Smith, W.H.F., 1996. A global, self-consistent, hierarchical, high-resolution

shoreline database. J. Geophys. Res. 101 (B4), 8741–8743. https://doi.org/10.1029/96JB00104.
Westerink, J.J., Luettich, R.A., Feyen, J.C., Atkinson, J.H., Dawson, C., Roberts, H.J., Powell, M.D., Dunion, J.P., Kubatko, E.J., Pourtaheri, H., 2008. A basin- to channel-scale unstructured grid hurricane storm surge model applied to Southern Louisiana. Am. Meteorol. Soc. 136 (3), 833–864. https://doi.org/10.1175/2007MWR1946.1.
Wolf, J., 2009. Coastal flooding: impact of coupled wave-surge-tide models. Nat. Hazards 49, 241–260. https://doi.org/10.1007/s11069-008-9316-5.
Wolf, J., 1981. Surge-Tide Interaction in the North Sea and River Thames. In: Floods due to High Winds and Tides. Elsevier, New York, pp. 75–94.
Xie, L., Bao, S., Pietrafesa, L.J., Foley, K., Fuentes, M., 2006. A real-time hurricane surface wind forecasting model: formulation and verification. Mon. Weather Rev. 134 (5), 1355–1370. https://doi.org/10.1175/MWR3126.1.
Zamudio, L., Hogan, P.J., 2008. Nesting the Gulf of Mexico in Atlantic HYCOM: oceanographic processes generated by Hurricane Ivan. Ocean Modell. 21 (3–4), 106–125. https://doi.org/10.1016/j.ocemod.2007.12.002.
Zhong, L., Li, M., Zhang, D.L., 2010. How do uncertainties in hurricane model forecasts affect storm surge predictions in a semi-enclosed bay. Estuar. Coast. Shelf Sci. 90, 61–72. https://doi.org/10.1016/j.ecss.2010.07.001.